NASA CONTRACTOR REPORT

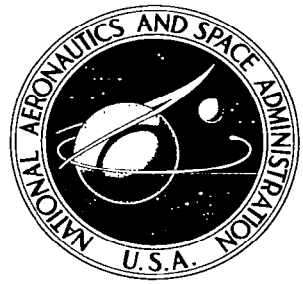

NASA CR-7

NASA CR-717

A LABORATORY PROGRAM TO DEVELOP IMPROVED GRAZING INCIDENCE X-RAY OPTICS

by T. Zehnpfennig, R. Giacconi, R. Haggerty, W. Reidy, and G. Vaiana

Prepared by
AMERICAN SCIENCE AND ENGINEERING, INC.
Cambridge, Mass.
for Goddard Space Flight Center

NATIONAL AERONAUTICS AND SPACE ADMINISTRATION • WASHINGTON, D. C. • FEBRUARY 1967

NASA CR-717

A LABORATORY PROGRAM TO DEVELOP IMPROVED GRAZING INCIDENCE X-RAY OPTICS

By T. Zehnpfennig, R. Giacconi, R. Haggerty, W. Reidy, and G. Vaiana

Prepared under Contract No. NAS 5-3992 by
AMERICAN SCIENCE AND ENGINEERING, INC.
Cambridge, Mass.

for Goddard Space Flight Center

NATIONAL AERONAUTICS AND SPACE ADMINISTRATION

For sale by the Clearinghouse for Federal Scientific and Technical Information
Springfield, Virginia 22151 – Price $2.50

ABSTRACT

The design and fabrication of grazing incidence double reflection optics is discussed. Tests, equipment, and laboratory techniques useful for the evaluation of these telescopes are described, and the properties of several fabricated telescopes are presented. A resolution of a few arc seconds has been obtained in visible light. X-ray measurements were limited by the available techniques, but the resolution measured at 8A is better than 30 arc seconds. Typical telescope double reflection efficiencies are on the order of 20% at 8A.

TABLE OF CONTENTS

TABLE OF CONTENTS (Cont'd)

LIST OF FIGURES

LIST OF FIGURES (cont'd)

1.0 INTRODUCTION

This document constitutes the final report prepared under Contract NAS 5-3992. The work performed under this contract was directed to the design, development, fabrication, and test of high resolution, grazing incidence x-ray optics.

Section 2 of this report discusses in detail the design and theoretical limitations on the resolution and reflection efficiency. In addition, the results of a ray tracing program are presented; and based on this, the telescope resolution, as a function of the angular deviation of the object from the optical axis of the telescope, is determined.

Section 3 describes in detail the two fabrication processes that were used in the program: that of electroforming a mirror on an optically polished mandrel and that of directly polishing the internal surfaces.

Section 4 discusses the tests and calibration techniques that were used to evaluate mirrors fabricated on this contract.

Section 5 gives the details of results that were obtained with these mirrors. The best mirror produced under this contract was directly fabricated by conventional optical methods. It consisted of a cast aluminum structure within which was deposited a thin layer of Kanigen, which served as the reflecting surface. The Kanigen surface was polished to the desired paraboloidal and hyperboloidal curves with an accuracy of one wavelength of visible light. Resolution of better than 5.0 arc seconds in visible light has been obtained with this mirror. The telescopes produced using the electroforming process are conical approximations to the desired curves. The resolution obtained with these devices was an order of magnitude poorer than that obtained with the Kanigen telescope. Typical measures of the telescope efficiency for x-rays at 8A give a value of 20%, which is approximately 30% of the theoretical value. (It is believed that the remaining

70% strikes local irregularities on the reflecting surfaces. This causes it to be absorbed, or to be reflected with a sufficient angular error to miss the image area.)

Tests to determine the effect of vacuum environment or temperature variation on these devices show that there was no degradation of the reflection efficiency in a vacuum environment and no permanent distortion of the mirror surface in thermal cycling, if the devices were properly mounted. Initial thermal testing showed permanent strains could be introduced into the mirror by the differential thermal expansion of the holding assembly, if the holding assembly was not carefully designed.

The New Technology Report pertaining to this contract has been prepared and submitted under American Science and Engineering document No. ASE-1148 in accordance with the contract's New Technology clause.

2.0 Telescope Design and Performance Calculations

In this section, a procedure for the optical design of x-ray telescopes is presented, along with calculations of reflection efficiency, angular resolution and image intensity distribution. These calculations were performed to evaluate the designs of the telescopes made under this contract, and to clarify certain aspects of their observed performance. However, they are sufficiently general to be of value in work involving other designs and other types of grazing incidence optical systems.

2.1 Telescope Design

The use of paraboloidal mirrors at grazing incidence as x-ray telescopes was first proposed by Giacconi and Rossi [1]. The optical design of such systems has been greatly improved by the use of two reflecting surfaces, following the design of Wolter [2]. Early development of the device is summarized by Giacconi et al in "Aplanatic Telescope for Soft X-rays". [3]

Each of the x-ray telescopes constructed under this contract consists of an internal paraboloidal reflecting surface and an internal hyperboloidal reflecting surface (see Fig. 2-1); or of conical approximations to these surfaces. The surfaces are co-axial and the focus of the paraboloid lies at the conjugate focus of the hyperboloid. The image of a distant source is formed on a surface passing through the focus of the hyperboloid after grazing angle reflections by the two mirror surfaces. The focal length F is the distance from the focus to the plane of intersection of the paraboloid with the hyperboloid. This geometrical configuration was chosen in preference to other possible combinations of reflecting surfaces because the deviations of the incident rays are inward, toward the optical axis, for both reflections. This maximizes the product of efficiency and collecting area for a given telescope diameter and focal length.

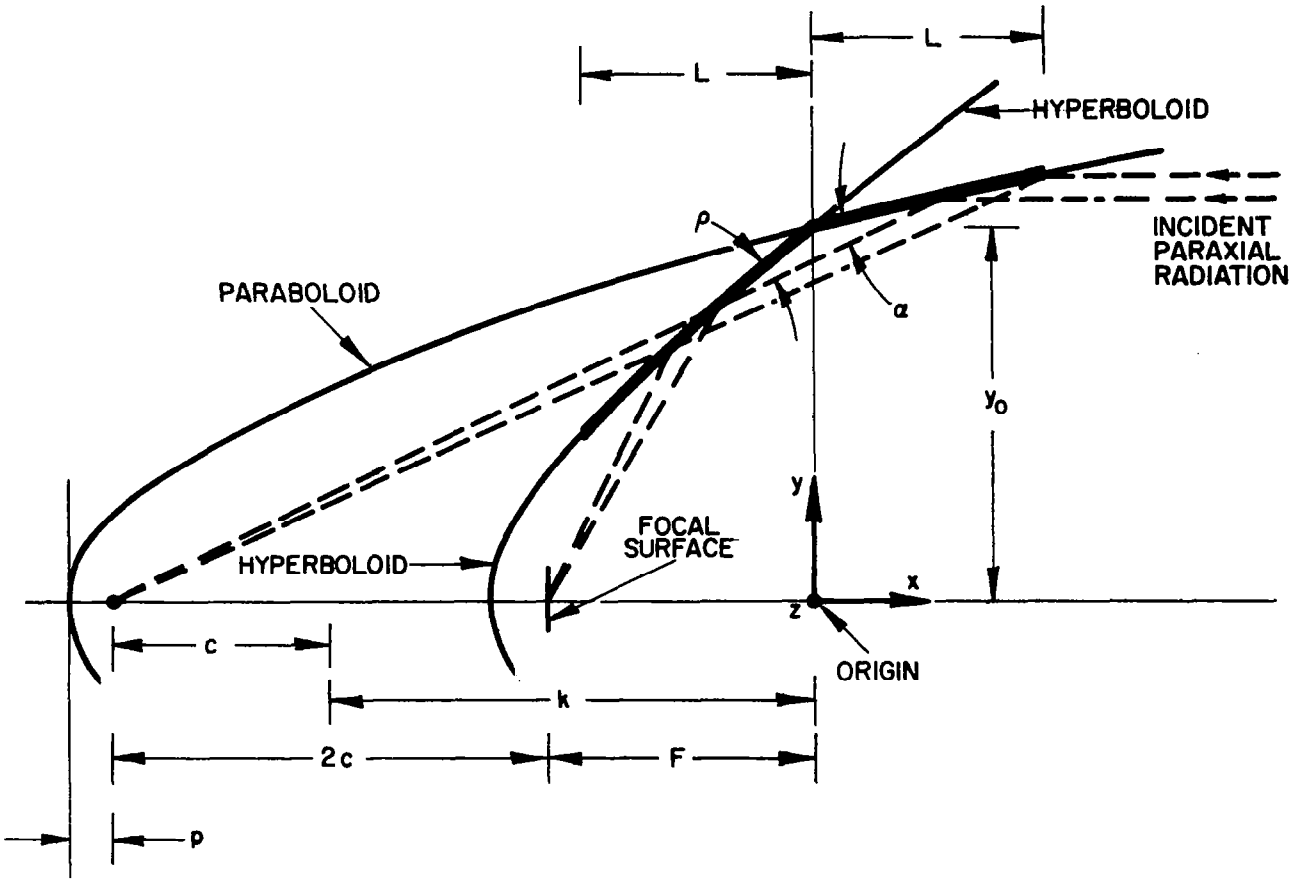

Fig. 2-1

SCHEMATIC CROSS-SECTION OF AN X-RAY TELESCOPE

The general equations of a paraboloid and a co-axial, confocal hyperboloid, in the coordinate system of Figure 2-1, are:

$$\underline{\text{Paraboloid}} \qquad y^2+z^2=4p(x+p+c+K) \tag{2-1}$$

$$\underline{\text{Hyperboloid}} \qquad \frac{(x+K)^2}{h^2} - \frac{y^2+z^2}{c^2-h^2} = 1 \tag{2-2}$$

The four constants in these equations may be expressed entirely in terms of two initial design parameters F (focal length) and y_o (radius of the telescope surfaces in the plane x=o) if one constraint is applied to the slopes of the surfaces with respect to the optical axis. This constraint consists of specifying the relation between the angles α and ρ . Let α be the angle between the paraboloidal surface and an incident, paraxial ray which strikes the paraboloid near the plane x=o. After reflection, this ray will strike the hyperboloid, also near the plane x=o. Let ρ be the angle between this ray and the local hyperboloidal surface. For telescopes designed and constructed under this contract, α was made approximately equal to ρ . The reason for this choice is to maximize telescope efficiency at short wavelengths. If, for instance, α were made smaller, then ρ would have to be increased for a given telescope diameter and focal length. Because of the well defined short wavelength cutoff exhibited by most prospective telescope materials at the grazing angles considered here (30 to 60 arc min.), an increase in ρ would necessarily decrease the effective wavelength range of the telescope at the short wavelength end. This argument applies similarly for a decrease in ρ . The optimum situation exists for $\alpha = \rho$.

An additional constraint is that α and ρ must be such that efficient grazing angle reflections will be obtained over the entire desired field of view. For a field of view of angular diameter b, the grazing reflections will lie within the following limits:

$$\begin{aligned} &\text{maximum grazing angles} \begin{cases} \alpha + \frac{b}{2} \\ \rho + \frac{b}{2} \end{cases} \\ &\text{minimum grazing angles} \begin{cases} \alpha - \frac{b}{2} \\ \rho - \frac{b}{2} \end{cases} \end{aligned} \tag{2-3}$$

Theoretical reflection efficiencies are calculated for various reflecting materials as a function of wavelength and grazing angle in Section 2. 2.

Since $\alpha = \rho$, then, referring to Figure 2-1, p can be found as follows:

$$4\alpha = \tan^{-1}\left(\frac{y_0}{F}\right) \approx \frac{y_0}{F} \tag{2-4}$$

The angle α may also be found from Equation 2-1:

$$\alpha = \left(\frac{dy}{dx}\right)_{x=0} = \frac{2p}{y_0} \tag{2-5}$$

Combining these expressions:

$$p = \frac{y_0^2}{8F} \tag{2-6}$$

The constant k, as can be seen in Fig. 2-1, is just:

$$k = c + F \tag{2-7}$$

The constant c can be found by realizing that paraxial rays reflected from the paraboloid are sent toward its focus. Therefore:

$$2c + F = \frac{y_0}{\tan 2\alpha} \approx \frac{y_0}{2\alpha} \tag{2-8}$$

Combining Equations 2-4 and 2-8:

$$c = \frac{F}{2} \tag{2-9}$$

Finally, h^2 may be found by requiring the paraboloid and hyperboloid to intersect in the plane x=o. The result is :

$$h^2 = \frac{1}{2}\left\{c^2+k^2+4p\left[p+c+k\right]-\left[\left(c^2+k^2+4p\left(p+c+k\right)\right)^2-4c^2k^2\right]^{1/2}\right\} \tag{2-10}$$

Equations 2-1, 2-2, 2-6, 2-7, 2-9, and 2-10, constitute the optical design for x-ray telescopes of this geometrical configuration, with the constraint $\alpha = \rho$. Because of the approximations that were made, α will not be precisely equal to ρ . The surfaces will, however, be exactly confocal.

When the parameter L, the length along the axis of each of the reflecting surfaces, is introduced, the collecting area and f-number of the system can be calculated:

$$\text{collecting area} = \frac{\pi y_0^2 L}{2F} \tag{2-11}$$

$$f\text{-number} = \frac{F}{y_o}\left(\frac{F}{2L}\right)^{1/2} \qquad (2\text{-}12)$$

The f-number, as written in Equation 2-12, does not, of course, take into account the reflection efficiency of the telescope surfaces.

2.1.1 Conical Approximations to the Paraboloid and Hyperboloid

When permitted by the desired performance level of the telescope, conical approximations to the paraboloid and hyperboloid can be used. For the conical telescopes designed under this contract, a given surface was approximated by the cone which was tangent to it midway along its length. Thus, to approximate a paraboloid, the radius y_1 of the paraboloid in the plane $x = +L/2$ was found. The slope of the paraboloid in this plane is:

$$\left(\frac{dy}{dx}\right)_{x=\frac{L}{2}} = \frac{2p}{y_1} \qquad (2\text{-}13)$$

Thus, the equation of the cone is:

$$(y^2+z^2)^{1/2} = \frac{2p}{y_1}\left(x-\frac{L}{2}\right)+y_1 \qquad (2\text{-}14)$$

The approximation to the hyperboloid was made similarly. The focusing performance of conical systems is discussed in Section 2.4.

2.1.2 Aperture Plates

In order to prevent direct or singly reflected rays from reaching the image area of the focal surface, circular aperture plates are normally placed in the planes $x = +L$ and $x = -L$. Originally, the diameter of the front aperture plate (at $x = +L$), was made equal to $2\,y_o$, the diameter of the reflecting surfaces in the plane $x = o$. Thus, a paraxial ray striking the paraboloid near $x = o$ would just graze the edge of the front aperture plate. The diameter of the rear aperture plate was chosen similarly: so that this same ray, after reflection from the paraboloid and the hyperboloid would just graze its edge. Aperture plates made to these dimensions are designated as full-sized aperture plates. Ray tracing programs showed that full-sized aperture plates were contributing significantly to vignetting, or the decrease

in effective collecting area at the edges of the field of view. Also, telescopes were often tested satisfactorily with no aperture plates at all, or with just a small disk to shadow the center of the focal surface from direct rays. Consequently, the following expressions for aperture plates of reduced diameter have been adopted:

$$d_1 = 2\gamma_0 - bL \tag{2-15}$$

$$d_2 = 2\gamma_0\left(1 - \frac{L}{F}\right) - bL \tag{2-16}$$

where d_1 and d_2 are the diameters of the front and rear aperture plates, respectively; and b is the angular diameter of the desired field of view.

2.2 Reflection Efficiency Calculations

In order to have at hand a convenient reference for calculating the theoretical reflection efficiency of telescope designs at various wavelengths in the soft x-ray range, a series of reflection efficiency curves was calculated using Fresnel's Equation [4]. These curves, shown in Figure 2-2 through 2-5, give the theoretical single-reflection efficiency as a function of wavelength, at various grazing angles, for four potential telescope materials: beryllium, aluminum, nickel, and gold. A form of Fresnel's Equation is the following:

$$\text{efficiency} = I/I_0$$

$$= \frac{\left\{2x - \left[\left((x^2-1)^2+y^2\right)^{1/2} + (x^2-1)\right]^{1/2}\right\}^2 + \left[(x^2-1)^2+y^2\right]^{1/2} - x^2 + 1}{\left\{2x + \left[\left((x^2-1)^2+y^2\right)^{1/2} + (x^2-1)\right]^{1/2}\right\}^2 + \left[(x^2-1)^2+y^2\right]^{1/2} - x^2 + 1} \tag{2-17}$$

where:

$$x = \frac{\theta}{\theta_c} = \left(\frac{\theta}{2\delta}\right)^{1/2} \tag{2-18}$$

$$y = \frac{\beta}{\delta} \tag{2-19}$$

$$\beta = \frac{(\mu/\rho)\rho\lambda}{4\pi} \tag{2-20}$$

$$\delta = \frac{e^2\lambda^2 N\rho}{2\pi mc^2 A} Z_A \tag{2-21}$$

(for wavelengths far from absorption edges)

$$\delta = \frac{e^2\lambda^2 N\rho}{2\pi mc^2 A}\left[Z_A + Z_H \frac{\lambda^2}{\lambda_H^2} \ln\left(\mp 1 \pm \frac{\lambda_H^2}{\lambda^2}\right)\right] \tag{2-22}$$

(for wavelengths near an absorption edge H)

THEORETICAL REFLECTION EFFICIENCY FOR BERYLLIUM

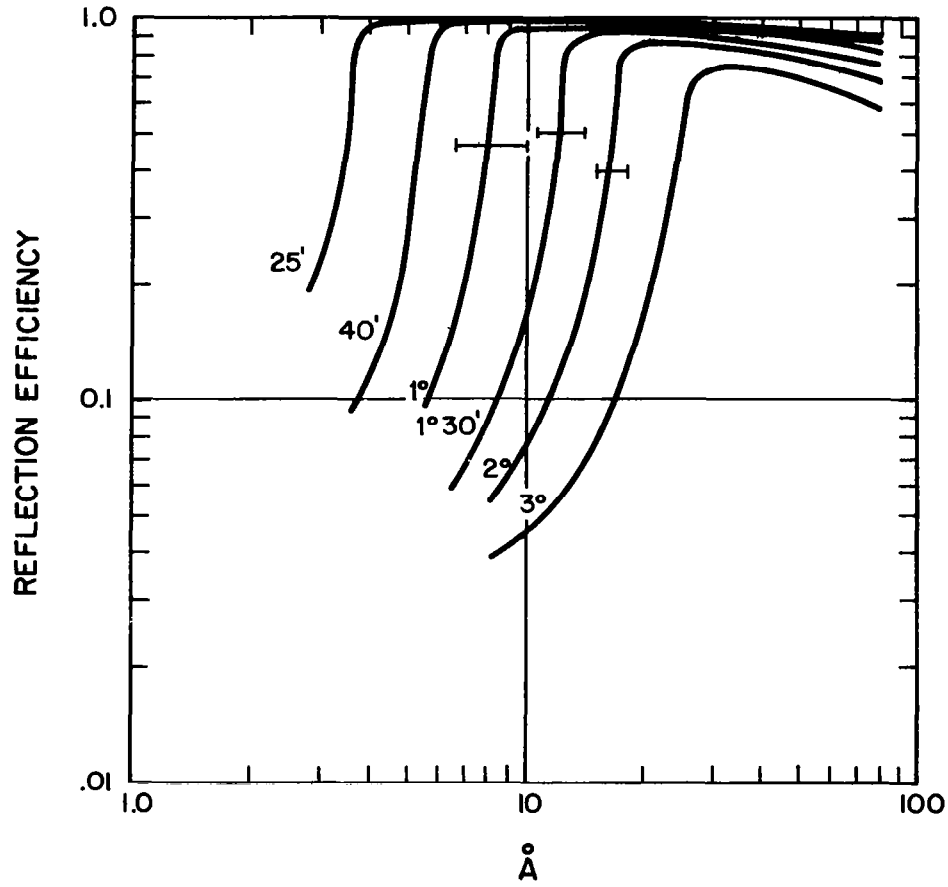

Fig. 2-2

THEORETICAL REFLECTION EFFICIENCY FOR ALUMINUM

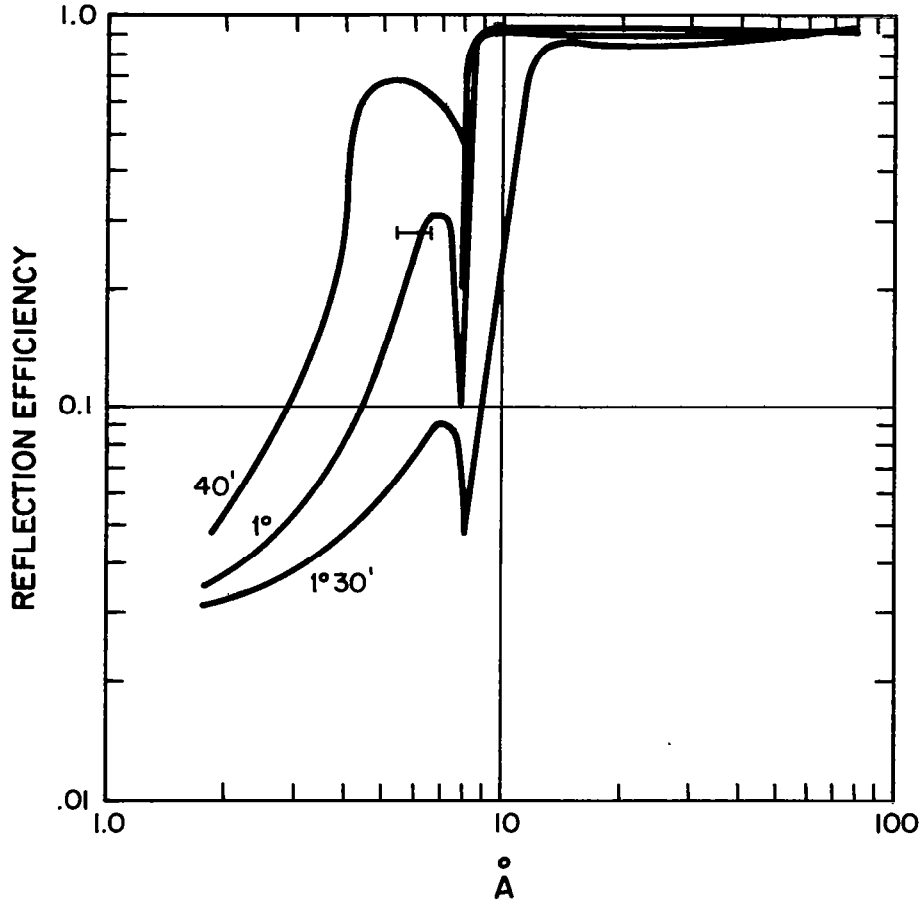

Fig. 2-3

THEORETICAL REFLECTION EFFICIENCY FOR NICKEL

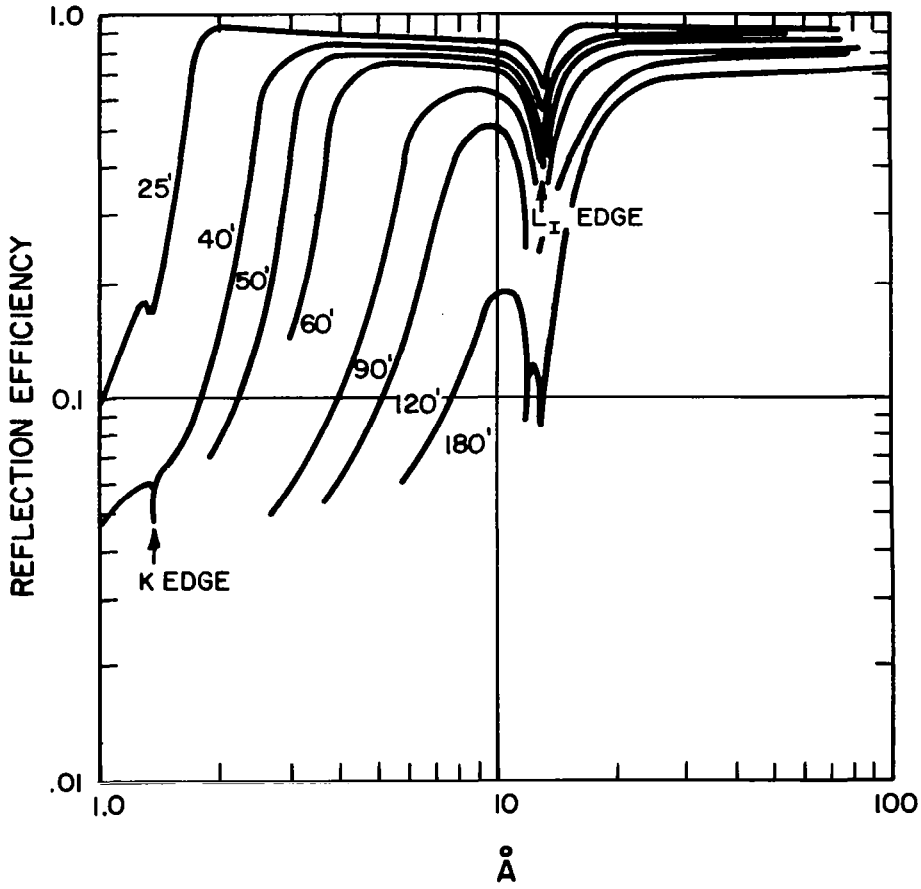

Fig. 2-4

THEORETICAL REFLECTION EFFICIENCY FOR GOLD

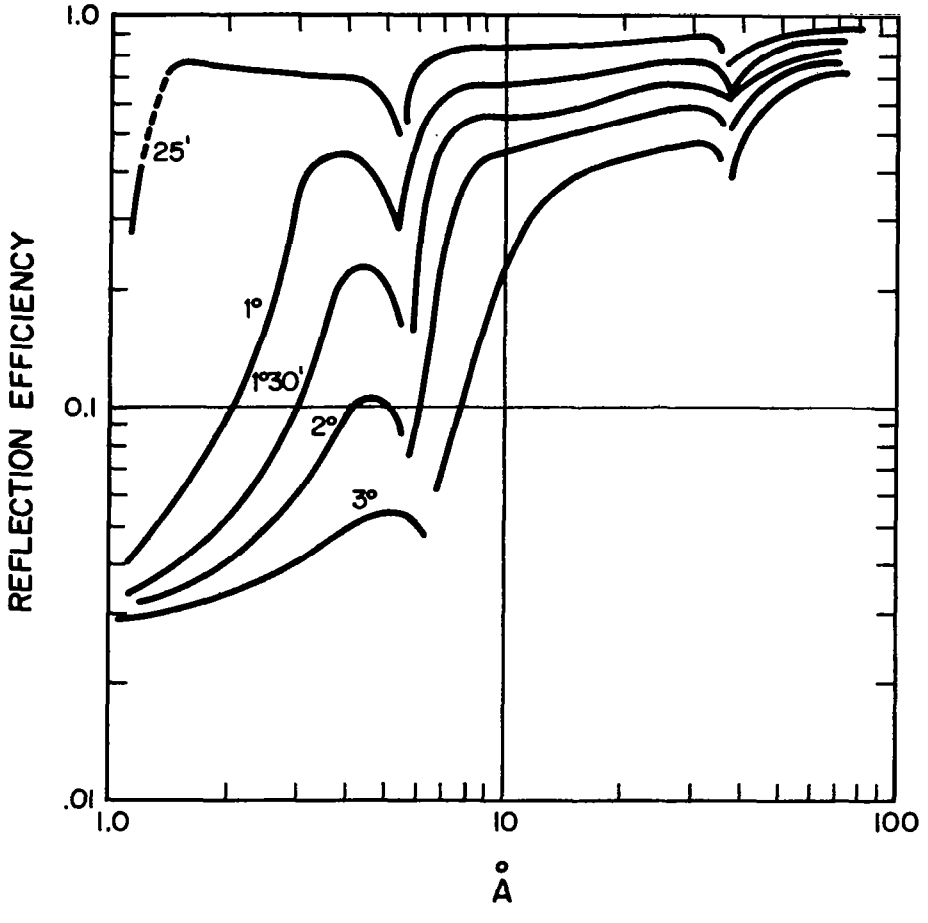

Fig. 2-5

Here:

θ = grazing angle of reflection

θ_c = critical angle of reflection

δ = unit decrement of the index of refraction

β = imaginary part of the index of refraction

μ/ρ = mass absorption co-efficient. (The values given by Henke [5, 6], were used)

ρ = density of reflecting material

λ = wavelength of incident radiation

e = electronic charge

N = Avagadro's number

m = electron mass

c = speed of light

A = atomic weight of reflecting material

Z_A = total electrons in the shells whose ionization potentials are less than hc/λ

Z_H = number of electrons in a given shell H.

λ_H = wavelength of the absorption edge H

The resulting curves showed that electron density should not be the only criterion used in evaluating a potential reflecting material. For, although, at a given grazing angle θ, a gold surface can reflect efficiently at shorter wavelengths than a beryllium one (because of the latter's short wavelength cutoff), at wavelengths longer than the cutoff, a beryllium surface is more efficient. Also, the curves show that the performance of a reflecting system at certain wavelengths can be strongly affected by a nearby absorption edge.

2.3 Ray Tracing Programs

In order to evaluate the imaging properties of a given x-ray telescope design, a ray tracing program was devised. This program is exact, and is capable of tracing skew rays. An outline of the program was presented previously [7], and is included in Appendix A.

This program was used to evaluate the optical design of the Kanigen telescopes described in Section 3. 2. Two successful computer runs were made: one for a planar focal surface normal to the optical axis and passing through the focus of the hyperboloid; and the other for a curved focal surface. For both runs, parallel bundles of sixty rays, each striking at a different point on the entrance aperture, were traced through the system at each of five angles of incidence to the optical axis: 0, 5, 10, 15, and 20 arc minutes. The coordinates of the intersections of these rays with the focal surface were printed out, and these intersections, or striking points, were plotted to produce diagrams such as Figure 2-6. This diagram, which will be called a blur circle plot, is for a parallel bundle of rays incident on the entrance aperture of the telescope at an angle of 5 minutes from the optical axis and imaged on a flat focal surface. From the asymmetry of the plot, the striking points of three rays are obviously missing. These are rays which struck the paraboloid but missed the hyperboloid. Along with the coordinates of the striking points, the computer also printed out the value of a function which helped to locate and eliminate such rays.

When the five blur circle plots for a planar focal surface were completed, the striking points of various rays in the focal plane were compared with their original points of incidence on the entrance aperture. From these correlations, it was seen that the radius r_o of each of the blur circles (except for paraxial rays) could be decreased by translating the focal plane slightly forward along the optical axis. However, the amount of translation required to minimize r_o was different for each blur circle, increasing with distance from the axis. Thus, the optimum focal surface was non-planar. The amount of translation needed to minimize the radius of each blur circle was plotted as a function of the distance of the corresponding blur circle from the axis. A good approximation to these points, it was found, could be made with the hyperboloid:

$$\frac{(x+28.7598)^2}{.00358} - \frac{y^2+z^2}{.0133} = 1 \qquad (2\text{-}23)$$

BLUR CIRCLE PLOT
(5 MIN. OFF AXIS)

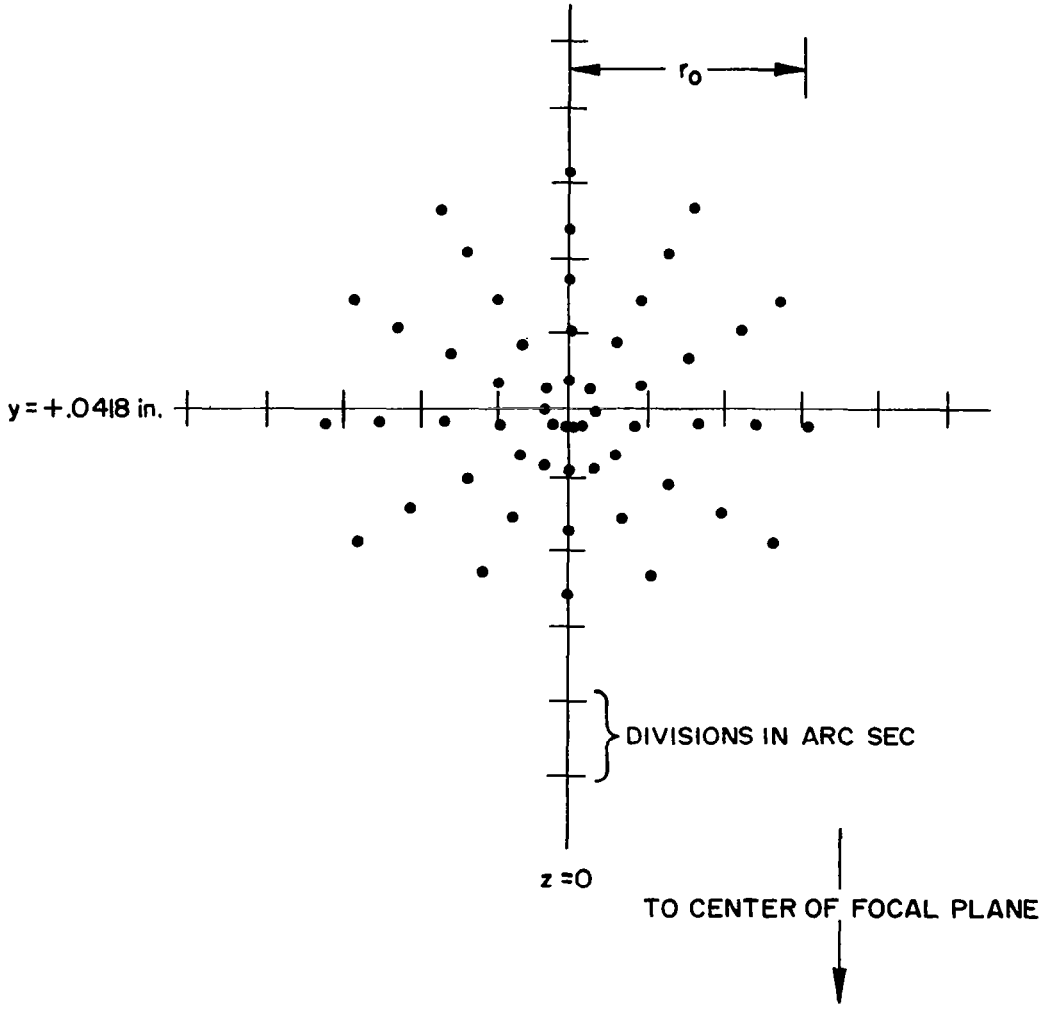

Fig. 2-6

CALCULATED BLUR CIRCLE RADII AND ANGULAR RESOLUTION

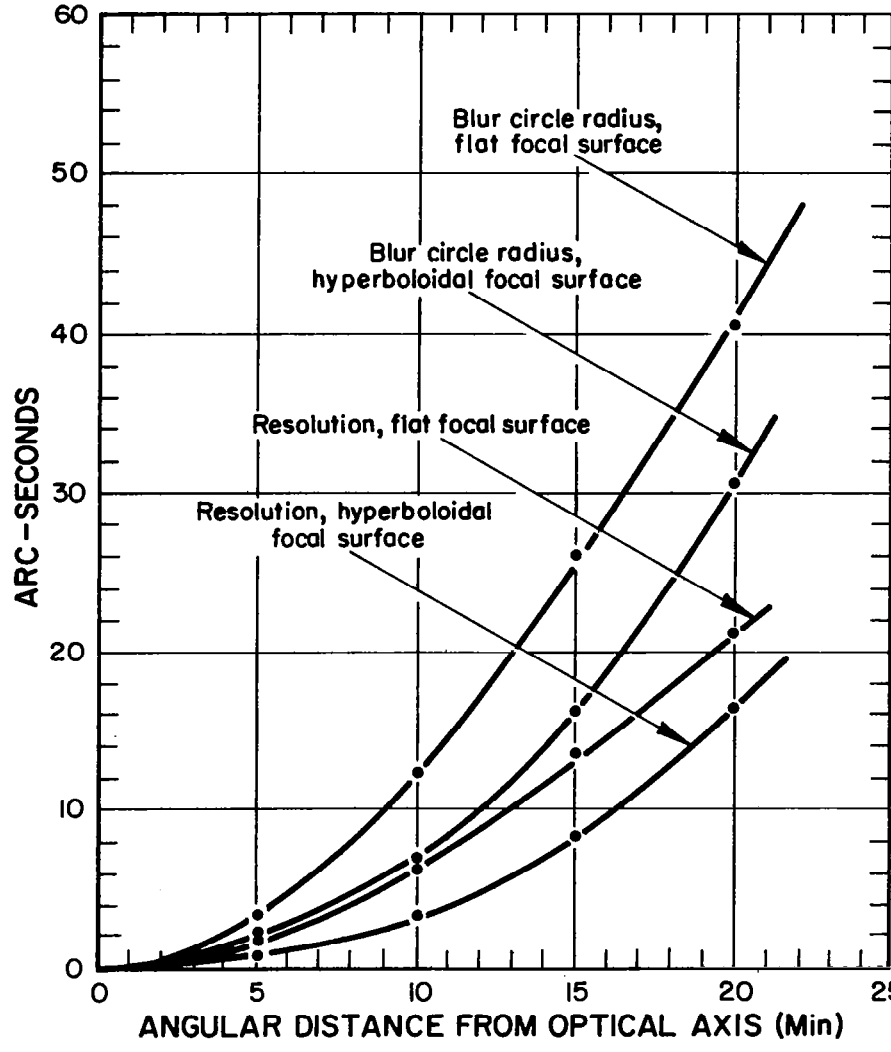

Fig. 2-7

This equation is written in the coordinate system of Fig. 2-1. Figure 2-7 shows the blur circle radii for the Kanigen telescope design of Equations 3-3 and 3-4 as a function of angle of incidence for a planar focal surface, and for the curved focal surface given by Equation 2-23. The curved focal surface is seen to be a factor of two improvement over the planar one near the center of the field of view.

In order to make a meaningful calculation of the angular resolution of a given telescope design, data on blur circle radii is not sufficient. In addition, the intensity distribution within the blur circle must be known. This information, however, may be found from blur circle plots such as Fig. 2-6. This is because of the fact that the incident rays were arranged to intersect the entrance aperture evenly over its area. Thus, each of the striking points in the plot can be considered to represent the same amount of incident energy. Therefore, the intensity at a location in the blur circle is proportional to the local density of these points. In Fig. 2-6, the points are arranged, approximately, in evenly spaced concentric circles about the center of the blur circle with the same number of points in each circle. Thus, the intensity within the blur circle goes as $1/r$, where r is the distance from the blur circle center. Outside the blur circle the intensity drops to zero. In Appendix B, a rather stringent definition of angular resolution is adopted, and the relation between blur circle radius and the angular resolution for the above intensity distribution is derived. This relation is:

$$\text{Angular resolution} = \frac{0.52\, r_o}{F} \qquad (2\text{-}24)$$

where r_o is the blur circle radius and F is the focal length. Angular resolution vs. angle of incidence for the Kanigen telescope design is plotted in Fig. 2-7. With the hyperboloidal focal surface, the diameter of the field of view for a theoretical resolution of 5 arc seconds is 24 minutes; that for 10 seconds is 33 minutes.

2.3.1 The Effect of Diffraction

In the preceeding discussion, the influence of diffraction on the image structure was not considered. An indication of the effect of diffraction may be obtained by calculating the radius of the first minimum in the diffraction pattern from a thin annular opening. From Born and Wolf [8], this is :

$$\theta_m = \frac{0.38\lambda}{y_o} \tag{2-25}$$

where λ is the wavelength of the incident radiation and y_o is the radius of the annulus (approximately 1.5 inches for the telescopes discussed here). Thus, θ_m = .002 arc seconds at 10A. Since abberations and fabrication tolerances limited the angular resolutions of the telescopes constructed under this contract to far larger angles than this, the effect of diffraction may be neglected in the soft x-ray range. At 5500 A, θ_m = 1.1 arc seconds; and thus, diffraction effects may slightly degrade the performance of the Kanigen telescope, described in Sections 3.2 and 5.2, in the visible range.

2.4 Image Formation with Conical Optics

In this section the imaging properties of x-ray telescopes consisting of perfect cones are discussed. This discussion is limited to regions near the center of the field of view. The procedure for approximating a given telescope design with conical surfaces was given in Section 2.1.1.

Figure 2-8 shows two paraxial rays in the x-y plane incident upon the surface of conical telescope. It can be simply proven that the spacing between such rays cannot be changed by reflections from the conical telescope surfaces. Thus, $\delta_1 = \delta_2$. Since the angle 4α is small, then : $\delta_1 = \delta_2 = \delta_3$. Because the maximum value δ_1 can take is equal to the annular opening αL, then the total diameter of the image of a distant point source positioned on the optical axis is also αL

The intensity distribution within the diameter αL may be found as follows. Consider a uniform bundle of collimated light incident on the telescope parallel to the optical axis. The locus of the rays after double

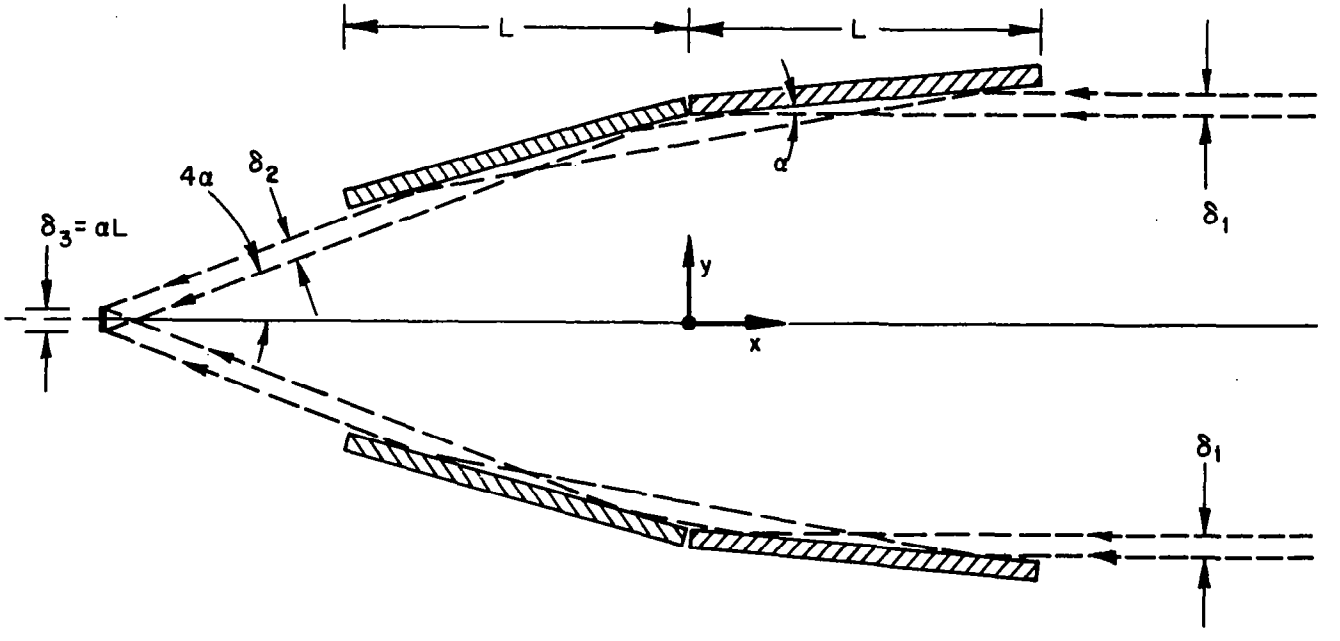

CONICAL OPTICS

Fig. 2-8

RESOLUTION OF A VISIBLE LIGHT TEST PATTERN WITH CONICAL OPTICS

CENTRAL PAIR OF SOURCES ARE SEPARATED BY 30 ARC SECONDS

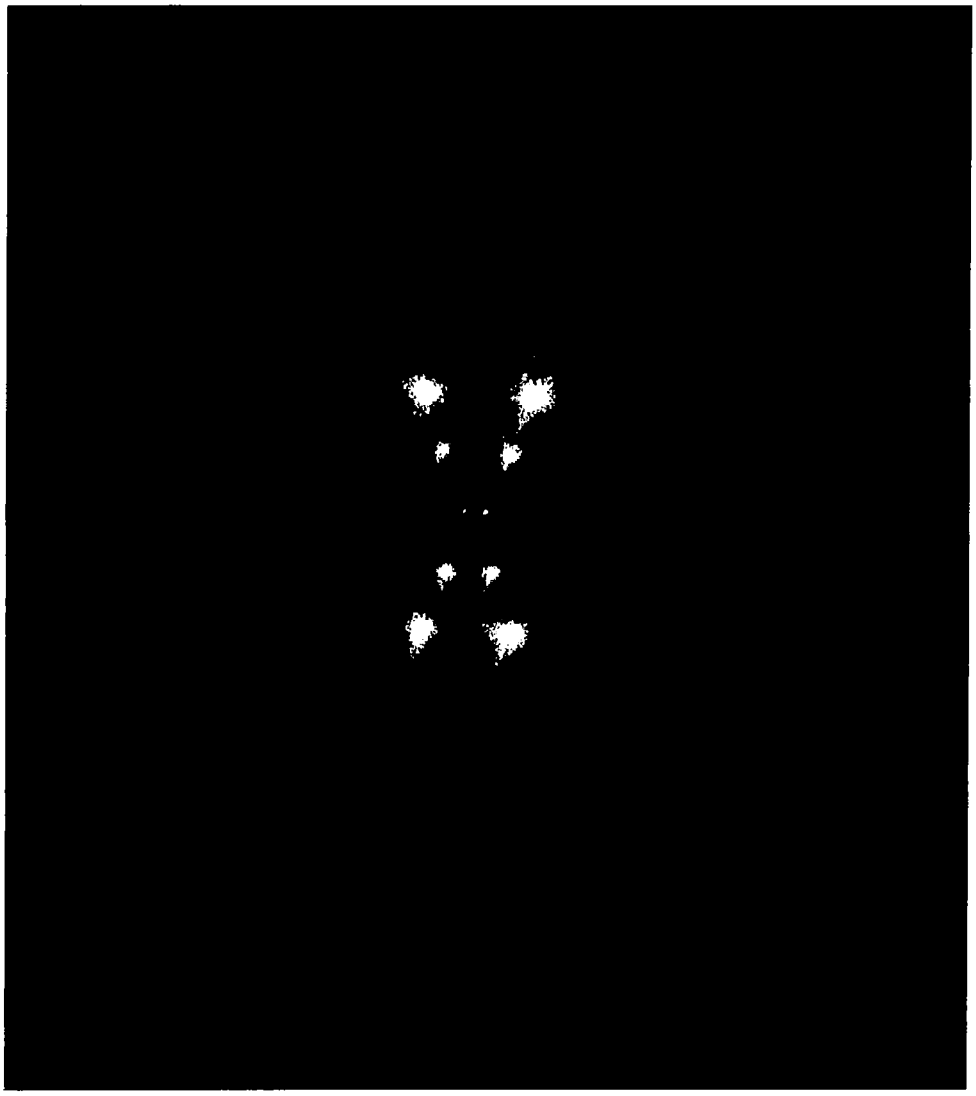

CQ-079

Fig. 2-9

reflection will be a hollow cone with a wall thickness of αL. In the focal plane, rays striking within a given differential ring ($2\pi R \Delta R$) concentric with the image center will have come from a given circular element of the telescope front reflecting surfaces. Therefore, all differential rings in the image area will contain equal flux:

$$\left.\begin{array}{l} I(R)2\pi R\Delta R = \text{constant} \\ I(R) \sim \frac{1}{R} \end{array}\right\} \text{for } R \leq \alpha \frac{L}{2}$$
$$I(R) = 0 \text{ for } R > \alpha \frac{L}{2} \qquad (2\text{-}26)$$

where I(R) is the intensity in the image as a function of the distance R from the image center.

Although this discussion was limited to sources on the axis, it also applies to the region near the axis where the effects of other abberations and vignetting are negligible.

Because the intensity profile in the image of a distant point source goes as 1/R, the angular resolution of conical telescopes for such sources should be much better than would be expected from the diameter αL of the total image. Indeed, neglecting diffraction, there should be no limit to the ability of a perfect conical system to resolve point sources. Fig. 2-9 is a photograph of a group of small sources taken with an electroformed conical telescope of the type described in Section 3.1. For this telescope, αL is .034 in., corresponding to an angle of 3.5 arc minutes in the focal surface. However, the closest pair of sources in the pattern, only 30 arc sec. apart, are easily resolved; and the diameters of the images of these two sources correspond to angles of only 10 arc seconds. It should be pointed out, though, that only a very small part of the energy collected by the telescope went into the effective image points. Most of it was spread over the total diameter αL of each image, and cannot be seen in this underexposed photograph. Thus, the actual efficiency of conical telescopes performing at this resolution level is very low.

Angular resolution, as defined in the appendix, can be calculated for conical telescopes. Using Equation B-4 from Appendix B and the parameters of the electroformed telescope design, the calculated angular resolution is 55 arc sec.

The intensity distribution for a circular source which is too large to be considered a point (that is, a source whose angular diameter is not small compared to $\alpha L/F$) can be found from a convolution integral. Consider a distant circular source of uniform intensity. If a perfect focussing system were used to form an image of this source, it would appear as the area S in Figure 2-10. Let $rdrd\theta$ be an element of this image. If the perfect system is now replaced by a conical one, the flux that was sent into the element $rdrd\theta$ will be spread out into the intensity pattern given by Equation 2-26. The total intensity at any selected point P in the focal surface can be found by adding the contribution at P of all the image elements in the area S. (Of course, those elements whose distance from P is greater than $\alpha L/2$ will not contribute). Thus:

$$I(P)=\int_S \frac{I_o}{r} rdrd\theta = I_o \int_S drd\theta \tag{2-27}$$

where I_o is a constant

If the point P is outside S, but the distance from P to any part of S is less than $\alpha L/2$, then Equation 2-27 becomes:

$$I(P)=2I_o\int_n^m \int_t^v drd\theta \tag{2-28}$$

where:

$$m=\sin^{-1}\left(\frac{R_o}{d}\right)$$

$$n=0$$

$$v=d\cos\theta+(R_o^2-d^2\sin^2\theta)^{1/2}$$

$$t=d\cos\theta-(R_o^2-d^2\sin^2\theta)^{1/2}$$

d = distance from P to center of S

R_o = radius of S.

This is an elliptic integral of the second kind. Thus:

$$I(P)=4I_oR_oE\left(\frac{d}{R_o},\sin^{-1}\frac{R_o}{d}\right) \tag{2-29}$$

$$=4I_oR_o\left[\frac{d}{R_o}E\left(\frac{d}{R_o},\frac{\pi}{2}\right)+\frac{R_o^2-d^2}{R_od}F\left(\frac{d}{R_o},\frac{\pi}{2}\right)\right]$$

INTEGRATION OVER A CIRCULAR SOURCE

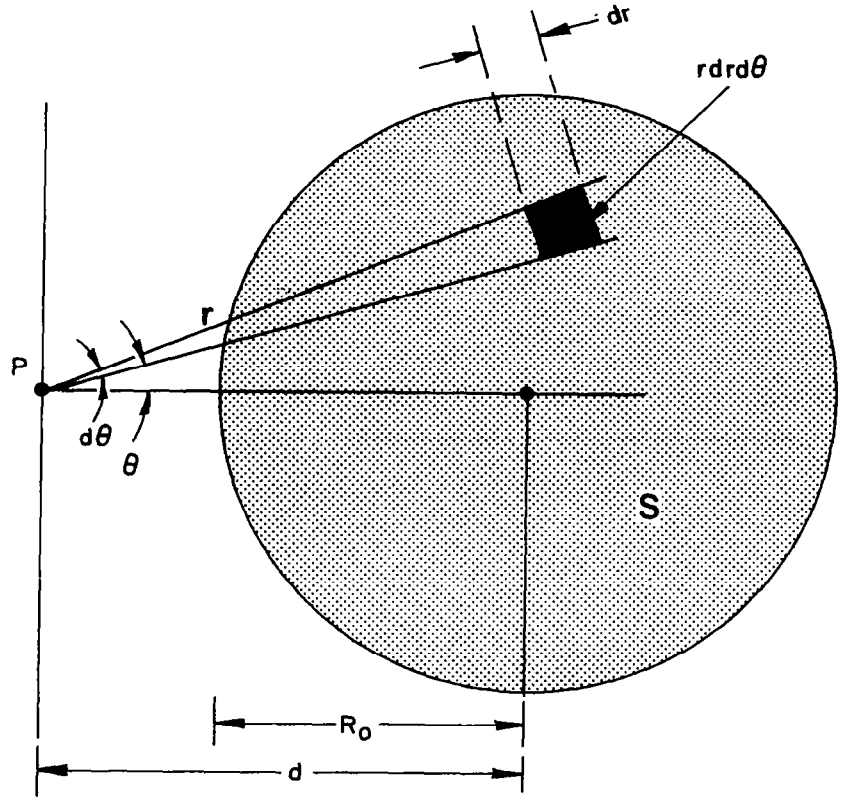

Fig. 2-10

INTENSITY PROFILES FOR THREE SOURCE DIAMETERS

$\left(\frac{aL}{F} = 3.5 \text{ MIN.}\right)$

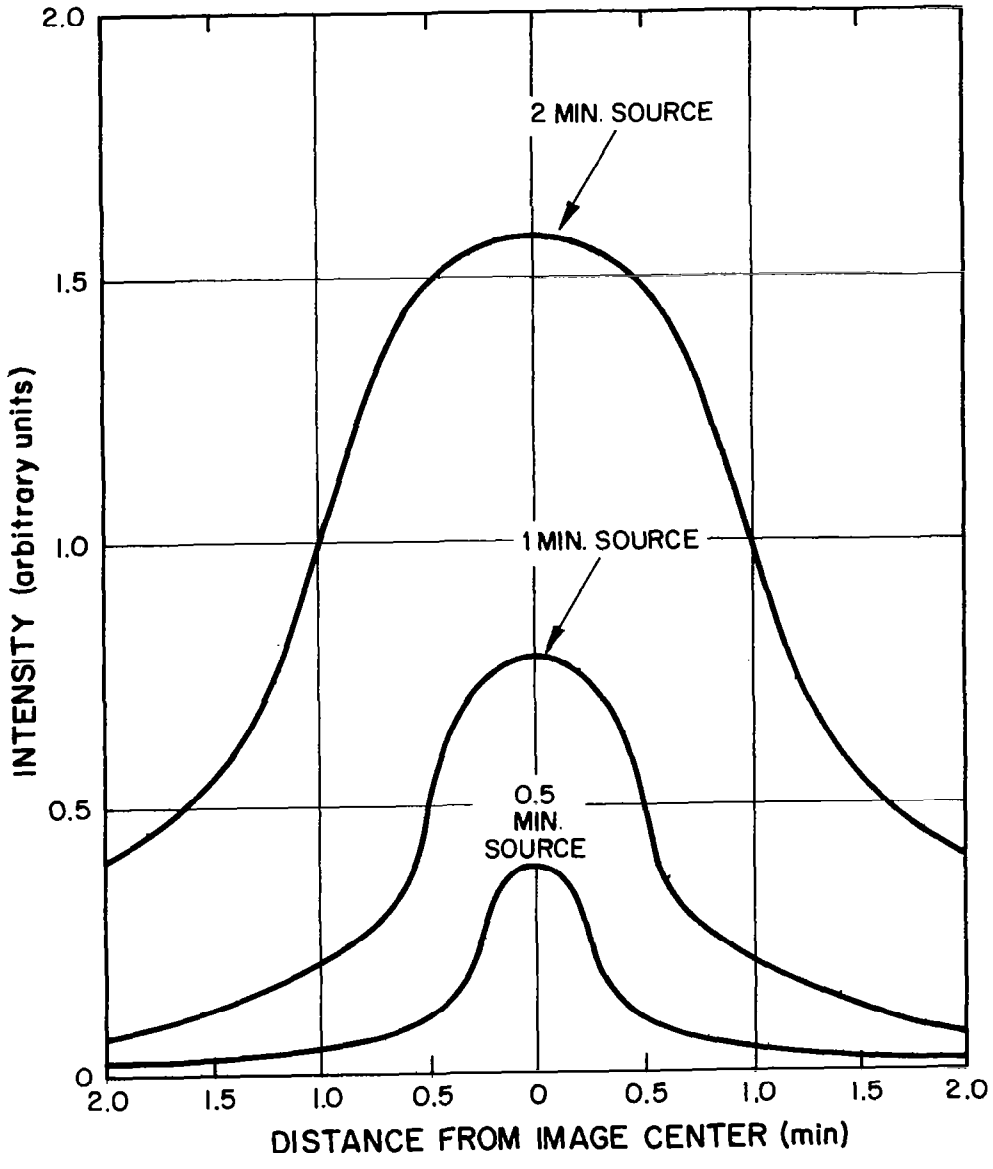

Fig. 2-11

where the functions E and F can be found in tables of elliptic integrals. The corresponding expression for point P within the boundary of S (that is, $d < R_o$) is:

$$I(P) = 2I_o R_o E\left(\frac{d}{R_o}, \pi\right) = 4I_o R_o E\left(\frac{d}{R_o}, \frac{\pi}{2}\right) \qquad (2\text{-}30)$$

When the value of I (P) is calculated from Equations 2-29 and 2-30 as a function of d, the intensity profile of the image of a source whose angular diameter is $\frac{2R_o}{F}$ is generated. Figure 2-11 shows the calculated intensity profiles for images of sources that were two, one and one-half arc min. in diameter. These sources were uniform and all three were of equal intensity (that is, equal flux per unit solid angle). Despite this, the peak intensity in the image decreases with source diameter. The telescope parameters used for this calculation are those of the electroformed nickel telescope described in Section 3. 1. The value of $\alpha L/F$ for these telescopes is 3. 5 arc min.

Note that Equations 2-29 and 2-30 apply only if all parts of S lie within a distance $\alpha L/2$ of the point P . For cases where this does not hold, more complicated limits of integration must be used in Equation 2-27.

As in Section 2. 3, the influence of diffraction has been neglected here, since the angular size of the diffraction pattern in the soft x-ray range , as given in Equation 2-25, is orders of magnitude smaller than the angular errors produced by abberations and typical fabrication tolerances.

3.0 Fabrication of the Telescopes

The x-ray telescopes were fabricated by two quite different processes: by electroforming on polished stainless steel mandrels; and by direct polishing of the telescope surfaces using conventional optical techniques. The electroformed telescopes are conical approximations to the proper paraboloidal and hyperboloidal shapes. The Kanigen telescope, named for the nickel alloy from which its reflecting surfaces are made, was polished to the proper shapes. Performance testing of these telescopes is reported in Section 5.0.

Electroformed telescopes of the design described here were flown on NASA Aerobee 4.63 GS from White Sands Missile Range on 17 March 1965, and obtained a group of soft x-ray pictures of the Sun [9].

3.1 Electroformed Nickel Telescopes

3.1.1 Design Considerations

The process of electroforming x-ray telescopes was developed in order to avoid certain problems associated with polishing internal surfaces to high tolerances. These problems are:

1. Internal surfaces cannot be supported on centers during grinding and polishing.

2. The design of automatic polishing devices is complicated by the requirement that they fit within such surfaces.

3. Autocollimators cannot conveniently be used in measurements of the local slopes of internal surfaces.

These problems were not severe or extremely restrictive, as is indicated by the successful fabrication of the telescope described in Section 3.2. Indeed, for the Kanigen telescope, these problems were not solved but avoided.

However, they were considered sufficiently compelling at the time when the first telescopes were fabricated on this program to make electroforming an attractive alternative. In addition, electroforming has the advantage that several identical telescopes can be made from a single mandrel.

The electroforming process of telescope fabrication, which is explained in detail in Section 3. 1. 3, consists of plating a thick (typically . 045 inch) layer of nickel on a polished stainless steel mold or mandrel. The outside surfaces of the mandrel were previously polished to the dimensions required of the internal surfaces of the telescope. The layer of nickel , which is the telescope, is separated from the mandrel by thermal shock.

Reasonable initial design parameters for the telescopes were considered to be a diameter of 3 inches, a length of about 3 inches for both reflecting surfaces, and an overall length from entrance aperture to focal surface of 36 inches. These dimensions were compatible with existing vacuum test facilities, as well as with flight packages into which these telescopes might be incorporated. Using the above dimensions in the telescope design equations of Section 2. 1, the following equations for the optical surfaces resulted:

$$\underline{\text{Paraboloid}} \quad y^2+z^2=0.0335779\,(x+63.9564) \quad \text{from } x=0 \text{ to } x=+3.052 \text{ in.} \tag{3-1}$$

$$\underline{\text{Hyperboloid}} \quad \frac{(x+48.4480)^2}{240.0054} - \frac{y^2+z^2}{0.24460}=1 \quad \text{from } x=0 \text{ to } x-2.948 \text{ in.} \tag{3-2}$$

These equations are written in the coordinate system of Fig. 2-1.

The telescopes which were electroformed under this contract were conical approximations to the above design. At the time when development of this fabrication method was begun, the angular resolution of the x-ray telescopes was limited by surface errors which were much larger than the difference between a given telescope design and its conical approximation. (This is about . 0001 in. for Equations 3-1 and 3-2). Thus, it was realized that substantial improvements in telescope performance could be achieved without the complication and expense of producing paraboloidal and hyperboloidal surfaces. Relevant characteristics of this design are

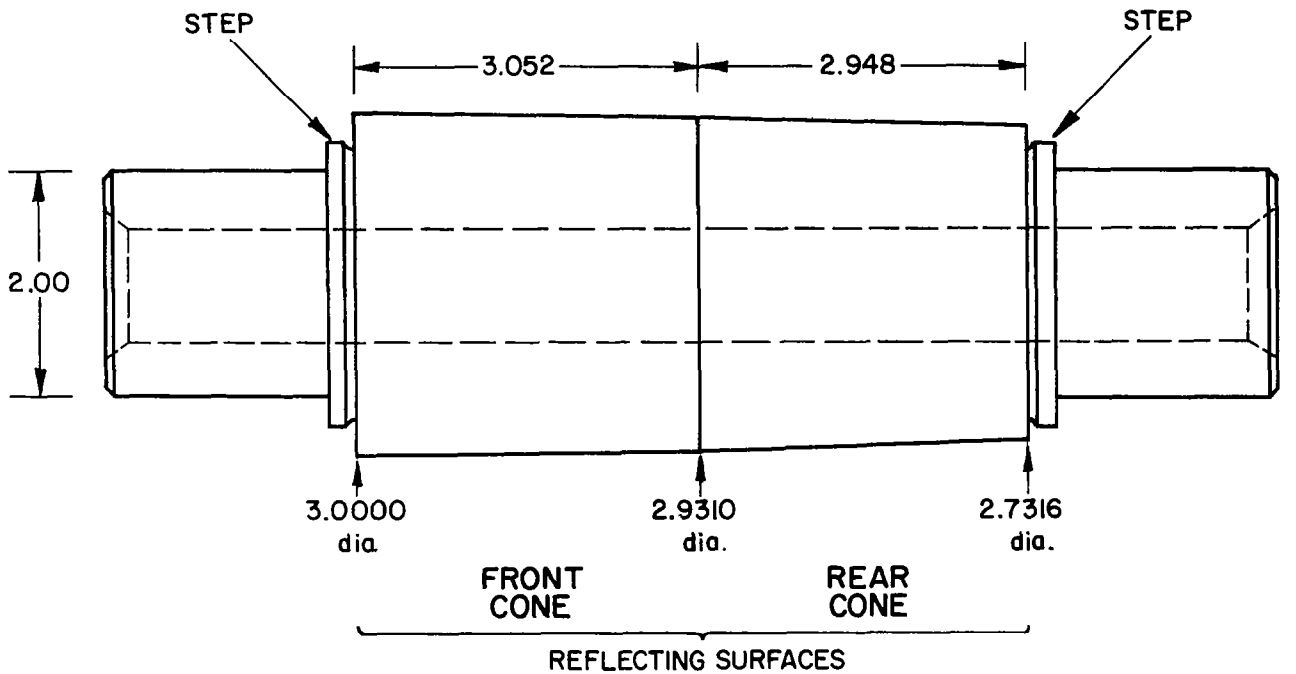

MANDREL

Fig. 3-1

listed below.

Diameters:

at x = +3.052 in.	3.000 in.
at x = 0	2.9310 in.
at x = -2.948 in.	2.7316 in.
Focal length	32.95 in.
Annular opening	0.034 in. (for full-sized aperture plates)
Collecting area	2.04 cm^2

Slopes of reflecting surfaces with respect to the optical axis:

front surface	0.0113 = 38.9 min.
rear surface	0.0338 = 116.2 min.

A computer printout of diameter vs. x, in increments of .025 inches, was produced and supplied to the mandrel fabricator.

3.1.2 Mandrel Fabrication

The electroforming method of telescope fabrication is worthwhile only if the telescope reflecting surfaces, upon removal from the mandrel, satisfy the design goals completely, without requiring additional shaping or polishing. If additional work is required, electroforming can only be considered to be an unnecessarily circuitous process. Thus, the mandrel must be machined and polished to tolerances equal or better than those required from the telescope.

Two mandrels were fabricated under this contract. Their mechanical configuration is shown in Figure 3-1. The dimensions in this figure are the original design values; the deviations of the finished mandrels from these values are discussed below. The reflecting surfaces (front cone and rear cone) are indicated in the figure. The other surfaces, which are discussed in Section 3.1.3, are used in connection with the electroforming operation. The material used was type 316L stainless steel, because of the fact that it can be polished to optical standards, and because it has a low carbon content and thus can be parted relatively easily from a nickel layer electroformed on it.

The mandrels were first machined to final dimensions with the exception of the reflecting surfaces. These were ground . 010 inches oversize in diameter. After being stress relieved, they were delivered to Frank Cooke, Inc., of North Brookfield, Massachusetts for final grinding and polishing. Here, the optical surfaces were precision ground on centers to very nearly the intended final dimensions. The two surfaces of each mandrel were then polished separately using diamond paste and various commercial polishing compounds. The polishing process consisted of rotating a mandrel slowly about its axis, while translating a small lap charged with the polishing compound back and forth over the surface by hand. Many lap materials were tried. The most effective ones were soft metals such as brass or lead. The only readily apparent defect in the final polish was a network of very fine scratches criss-crossing in the directions the lap most often moved across the mandrel surface.

In-process measurements of the optical surfaces were principally made with an air gauge. With this device, the change in diameter of a mandrel along its length could be measured within . 00005 in. Measurements were typically made at intervals of 0. 10 in. along the mandrel axis. By concentrating the polishing action in the regions where the measured diameter was too large, the surface profiles were made conical within about . 0002 in. The average slopes, as determined from the change in diameter over a length of two or three inches, were maintained within 30 arc seconds of the design values. The surfaces were kept round and concentric within . 0002 in. However, the absolute values of the diameters were more difficult to control. This was because material could be removed from a mandrel but not, of course, replaced; and because the probability that the mandrel surfaces would become highly polished, precisely conical, and of the proper slope at the same moment that the correct diameters were reached was quite low. Thus, the final polished surfaces were closely parallel to the designed surfaces, but displaced radially from them by up to . 003 in. The only noticeable effect

of these deviations was a slight change in focal length.

One persistent problem was the tendency of the nickel to stick to the steel at various points. This sticking or "wetting" of the surface caused small pits and protrusions when a telescope was removed from a mandrel. After a mandrel had accumulated surface defects from several telescope removals, its surface finish was usually restored by grinding and re-polishing. Because a small amount of material was removed by this process, the mandrels and the telescopes made from them eventually took on a variety of sizes. For instance, one of the mandrels described above was re-polished once, during which its diameter decreased by . 008 in. The variations in telescope performance resulting from these small changes are negligible.

The mandrel characteristic which most significantly limited the performance of the resulting telescopes was a prevalent small scale surface ripple. As measured, from the variable telescope calibrator data in Section 5.1.2, the slope errors involved were about one to two arc min. The probable cause of this ripple is the use of laps, during the mandrel polishing process, which covered only a small and localized portion of the mandrel surface at a time. The brass and lead laps which were applied to the rotating mandrel were in the form of flat bars. Thus, the zone of contact was a narrow line as long as the width of the bar, and this was never more than one inch. The narrow lap would tilt and wobble over local surface defects, whereas a lap which sampled a larger surface area could have removed them. A more effective lap geometry, shown in Figure 3-6a, was used for polishing the Kanigen telescope. Tilting of this lap due to a telescope surface defect of a given height is relatively small because of the large spacing and length of the two rigidly connected contact surfaces. Use of this lap probably contributed much to the superior performance of the Kanigen telescope.

3.1.3 Electroforming

The electroforming method of telescope fabrication was developed under this contract and under Contract NAS 5-3676. Nickel was chosen because, among those metals which can be electroformed using simple and predictable processes, it has a relatively low atomic number and a corrosion-resistant surface. An electroformed telescope is shown in Fig. 3-2.

To prepare a mandrel for the electroforming process, it is fitted with a pair of stainless steel end rings and a pair of insulating Delrin end caps. The end rings are held concentric to the mandrel axis by the cylindrical surfaces of the small steps seen adjacent to the reflection surfaces in Fig. 3-1. Because the diameter of each end ring is slightly larger than that of the adjacent reflecting surface, these rings determine the shape of the end faces of the telescope. The Delrin end caps fit closely over the two inch diameter cylindrical end sections of the mandrel, as well as over parts of the end rings and the support shaft. Their purpose is to insulate all parts of the assembly where plating is not desired. The threaded support shaft, which fits through the axial hole in the mandrel, holds the pieces of this assembly together.

The plating solution is contained in a 25 gallon polyester impregnated fiberglass tank. The mandrel assembly is held vertically, by its support shaft, from a holding fixture positioned above the tank. (See Fig. 3-3). A motor mounted on the holding fixture rotates the shaft and mandrel at about 7 rpm. (An attempt was made to electroform with no rotation, but the resulting nickel layer was not uniform.) Electrical contact is made with the mandrel assembly by two brushes which contact the support shaft above the surface of the plating solution. The nickel anodes are hung in the solution on two opposite sides of the tank near the walls. The electroforming current density near the mandrel surfaces is 10 to 20 amps per square foot.

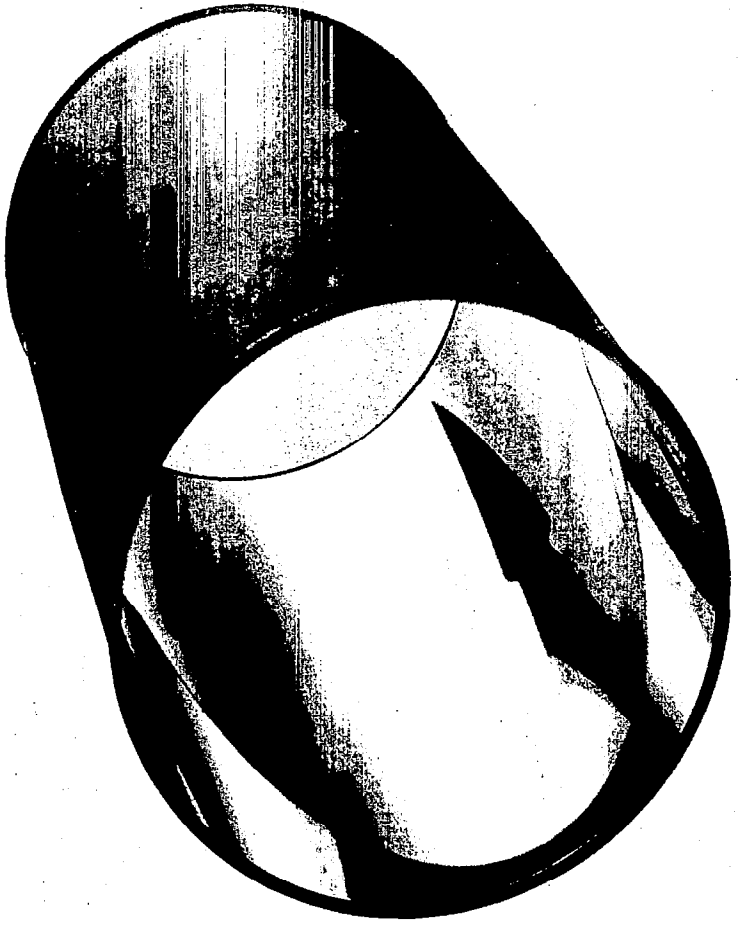

CD-096A

Fig. 3-2 AN ELECTROFORMED NICKEL TELESCOPE

ELECTROFORMING FACILITY

Fig. 3-3

Agitation and filtration are provided by a 150 gal. per hr. filter pump mounted in one corner of the tank. Solution temperature is maintained at 120° F by a thermostatically controlled immersion heater. Specific gravity, Ph, and surface tension of the solution are monitored periodically during the process, and any discrepancies are corrected by the use of additives. About 120 hrs. are required to electroform a telescope . 045 in. thick.

Nickel sulfamate plating solution was chosen in preference to other nickel plating solutions in order to achieve the lowest possible internal stress in the resulting deposition. Stress levels of about 500 psi are claimed by the manufacturers of these solutions. It is desirable to minimize internal stress in order to achieve optimum structural stability in the electroformed telescopes. Initially, a solution made by Meaker Co. was used. However, it was found that Type SN nickel sulfamate solution prepared by Barrett Chemical Products Co. gave more consistent and predictable results. Rolled depolarized nickel bars or depolarized nickel chips are used as the anode material. The chips are preferred because of their greater surface area and because nickel is removed from them more evenly.

An electroformed telescope is removed from its mandrel by thermal shock. The mandrel is held vertically, with its smaller end down. The axial hole in the mandrel is filled with liquid nitrogen and after about one hour, the telescope loosens and slips off. This technique produces less damage to the mandrel and telescope surfaces than the previously used method of forcing the telescope off in a mechanical press. Specifically, the pits and protrusions, produced in areas where the two pieces did not part precisely at the nickel-stainless steel boundary, are less frequent. Subsequent elongation of these defects, caused by the close sliding of the telescope over the mandrel surface when the pieces are forced apart, is also eliminated. Typically, four telescopes could be electroformed from a mandrel before its surface was considered unusable due to the density of these defects.

The replication of the mandrel surface was found to be detailed on a

REPLICATION OF DETAILS OF THE MANDREL SURFACE

TELESCOPE A

TELESCOPE B

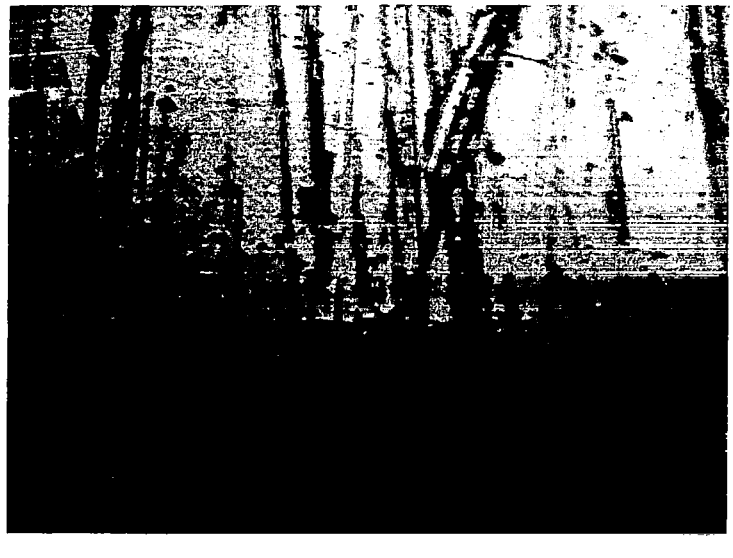

MANDREL

CQ-101

Fig. 3-4

very fine scale. Fig. 3-4 shows a scratched portion of a mandrel and the corresponding areas of two telescopes which were electroformed from it. The magnification of these photographs is 200X. The pattern of scratches is duplicated closely. Details as small as . 0001 in. are accurately copied. The large horizontal scratch evidently appeared after telescope A had been removed.

Because of the residual internal stresses and the forces applied during the removal operation, electroformed telescopes were typically found to be . 0005 in. out-of-round. Further distortions of up to . 003 in. T. I. R. could be induced by differential thermal expansion between the telescope and its mounting fixture. The out-of-roundness problem can probably be alleviated by increasing the wall thickness. This could be either done by additional electroforming or by building up the wall, before removal from the mandrel, with a process such as metal spraying. A telescope, which was already removed from its mandrel, was sprayed with . 025 in. of aluminum, to test the adherence of the layer. The adherence was satisfactory, and no additional strains were detected in the telescope.

3.2 The Kanigen Telescope

3.2.1 Design Considerations

As part of this program of x-ray telescope development, a second method of fabrication was pursued. A three inch diameter telescope was fabricated directly by lapping and polishing techniques similar to those used in producing conventional precision optical components. The principal advantages of this method over the electroforming process are as follows:

1. Materials may be used which are much more suited for optical fabrication than those available for use in the electroforming process.
2. The walls of the structure may be made arbitrarily thick and reinforcing ribs may be added, improving the structural stability of the telescope. The problem of mounting telescope to a holding structure without distorting it is considerably simplified by thick, rigid walls.

3. The stresses produced in the structure by the electroforming process and by removal from the mandrel are avoided.

This telescope was conceived primarily as a laboratory model, made to demonstrate the performance that could be expected when state-of-the-art optical fabrication techniques were employed. An on-axis angular resolution of 10 arc seconds was considered a minimum design goal. Fabrication of the paraboloid and the hyperboloid, instead of their conical approximations, was considered feasible with the fabrication techniques which were to be used. Therefore, this was incorporated into the design. The length of each reflecting surface was made approximately equal to its diameter (that is, 3 inches), in order to maximize the collecting area without producing internal surfaces which would be too long for convenient polishing. Because of the possibility that the telescope might be carried in an instrument package mounted on a bi-axial solar pointing control, its overall length was fixed at 31.7 in. to fit this package. Introducing these constraints into the equations in Section 2.1, the following design for the optical surfaces resulted:

Paraboloid $y^2+z^2=0.038160\,(x+55.96885)$ from $x=0$ to $x=+3.00$ in. (3-3)

Hyperboloid $\dfrac{(x+42.33295)^2}{185.4312}-\dfrac{y^2+z^2}{0.24650}=1$ from $x=0$ to $x=-3.00$ in. (3-4)

Some of the resulting dimensions of the reflecting surfaces are shown in Fig. 3-5. Additional parameters which can be derived from these equations are listed as follows:

Focal Length	28.7 in.
Collecting Area	2.3 cm^2

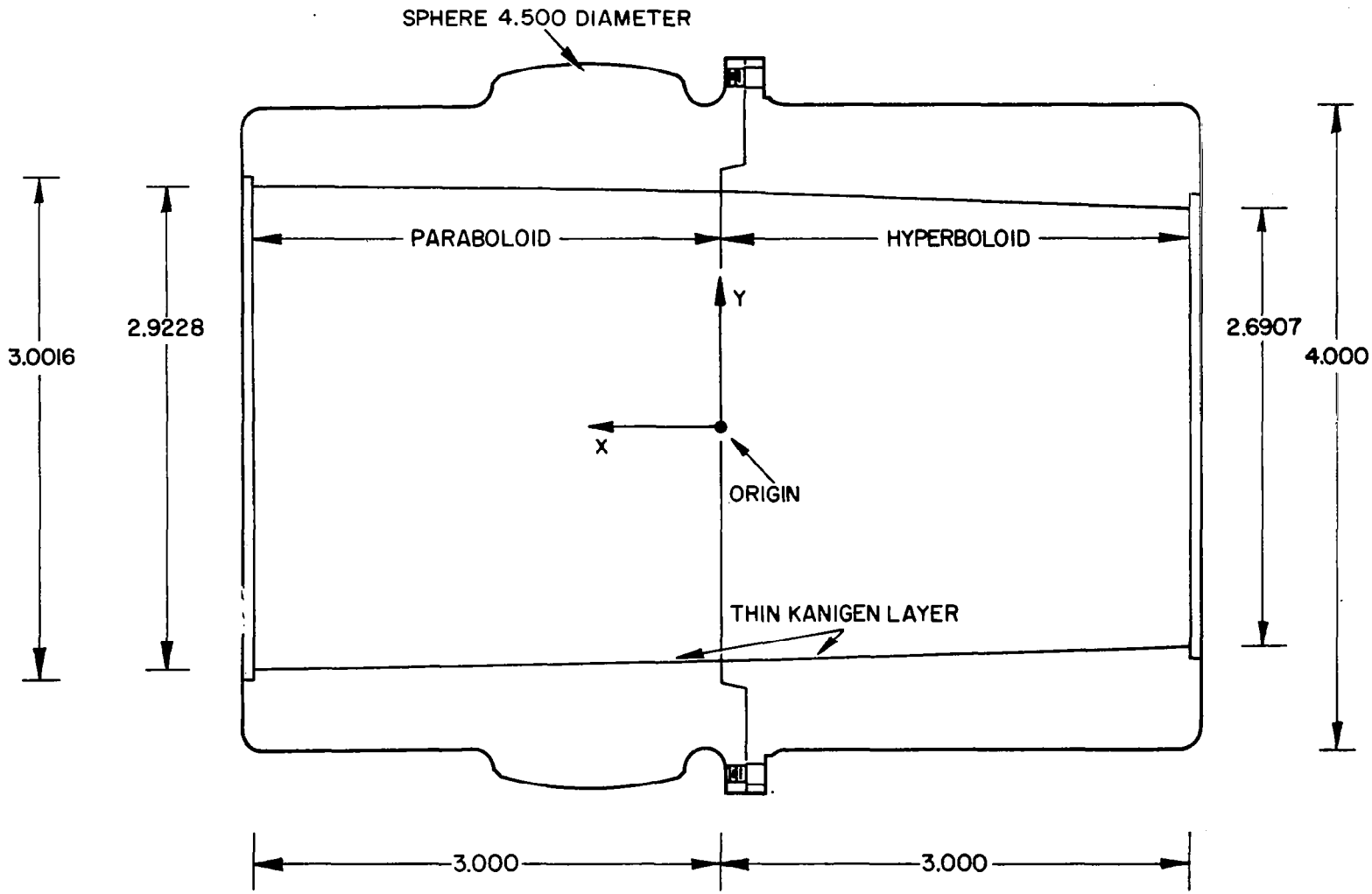

CROSS-SECTION OF KANIGEN TELESCOPE

Fig. 3-5

Slopes of reflecting surfaces with respect to the optical axis

paraboloid at x = +3.00 in.	0.012719 = 43.7 min.
paraboloid at x = 0	0.013056 = 44.9 min.
hyperboloid at x = 0	0.038507 = 132.4 min.
hyperboloid at x = -3.00 in.	0.038863 = 133.6 min.

Sagittal depths (departure from a cone)

paraboloid	0.000126 in.
hyperboloid	0.000133 in.

3.2.2 Fabrication of the Kanigen Telescope

Diffraction Limited, Inc., of Bedford, Massachusetts was chosen to fabricate this telescope. The fabricator was supplied with a set of specifications, a drawing of the mechanical configuration of the telescope, and a computer printout tabulating the diameter and slope of the optical surfaces as a function of x, in increments of .050 in. Instead of an imaging test in visible light, an acceptance test consisting of a series of mechanical measurements of diameters, slopes, and roundness, and an optical test of local surface profile was agreed upon. The reason for not employing an imaging test is that such a test would yield information on the overall surface accuracy alone, without specifying how closely each of the separate surface tolerances had been met. Also, the fabricator pointed out that imaging tests would not be useful to him in figuring the surfaces due to the narrowness of the annular ring, as viewed from the focal surface of the telescope. Thus, he would have to use measurements of diameters, slopes, and roundness in his in-processing testing.

The structural configuration of the telescope is shown in Fig. 3-5. Two mating aluminum castings support a thin layer of Kanigen, a chemically deposited alloy consisting of 90% nickel and 10% phosphorous. This material was chosen because of the fabricator's experience with it and because its polishing qualitites closely approach those of glass. Polishing and figuring of the optical surfaces were done entirely on the Kanigen layer.

The aluminum pieces were cast from Precedent 71A alloy and heat treated to achieve optimum structural stability. The castings were then machined to final dimensions on the outside, and approximately .005 in. oversize, on the diameter, inside. (The spherical surface shown in Fig. 3-5 is part of a contemplated ball-and-socket type mounting system.) The lengths of the castings along the axis were left oversize at this time so that the inevitable turned-down-edge could be machined off after the completion of optical polishing. Kanigen was then deposited on the inside surfaces to a depth of .005 in.

Lapping and figuring of the surfaces was done principally by hand. The paraboloidal and hyperboloidal sections of the telescope were lapped separately. The lap most frequently used consisted of a semi-cylinder of aluminum upon which two bars of pitch were mounted, as shown in Fig. 3-6a. The outside surfaces of the pitch bars made contact with the Kanigen surface of the telescope along narrow zones approximately parallel to the optical axis. Because of the geometries of the lap and the telescope, close contact could be maintained between the pitch surfaces and the Kanigen surface for axial rotations of the telescope and for translations of the lap along the optical axis within a range. Lapping consisted of coating the contacting surfaces with a slurry of commercial grinding or polishing compound, such as one of the Linde series, and moving the pieces repeatedly through a combination of the above rotations and translations. Because of the slow-flowing properties of the pitch, close contact was maintained despite changes in shape and wearing of the surfaces. Control of the Kanigen surface profile was achieved by standard optical figuring techniques: by control of lap pressure; by variations in length of the stroke; and by selective trimming and shaping of the lap surfaces.

In order to maintain a figure of revolution, another type of lap was occasionally used. Shown in Fig. 3-6b, this lap contacted about 50% of the optical surface at a time. The geometry of this lap permitted rotations only; it could not be translated along the optical axis. Work with this lap was done

POLISHING LAPS

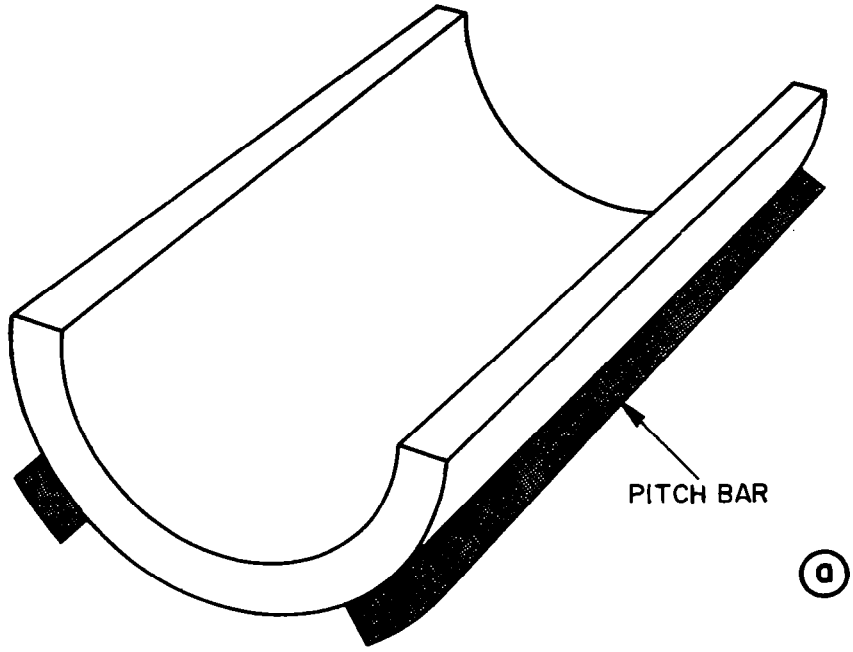

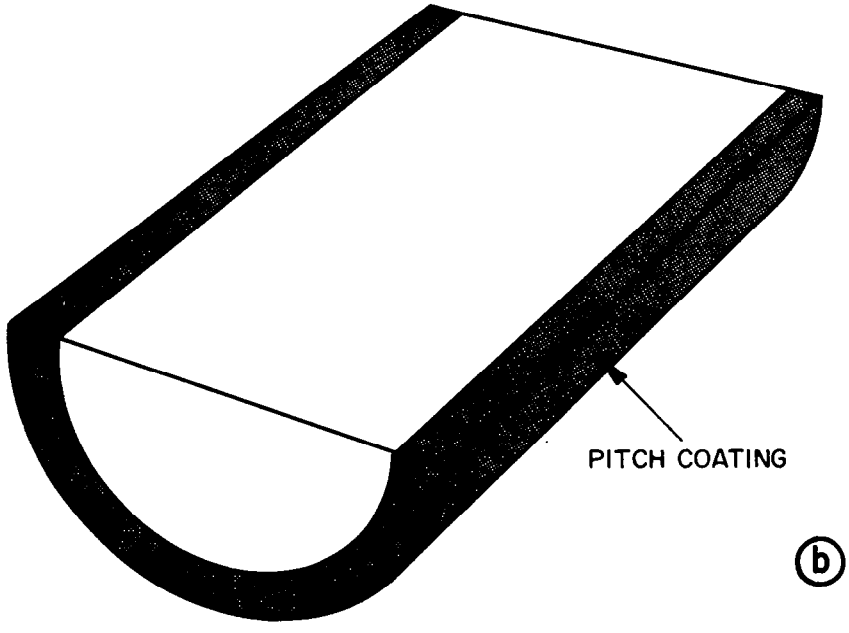

Fig. 3-6

TORROIDAL TEST PLATE

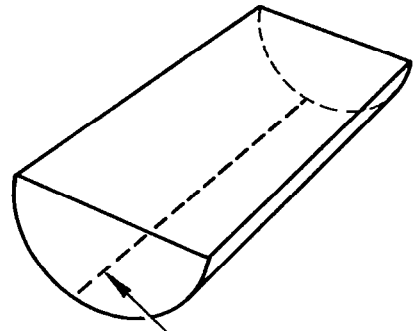

(a)

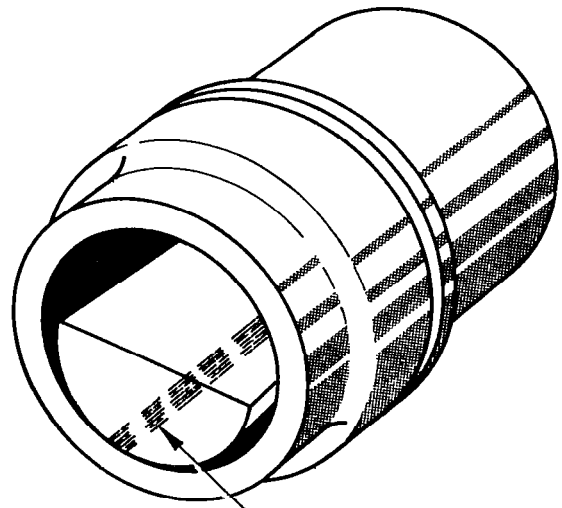

(b)

Fig. 3-7

by machine.

In-process testing was performed using air-gauges, precision height gauges, and a torroidal test plate. The air gauges were used to measure out-of-roundness of the surfaces. Any out-of-roundness greater than .00002 in. could be detected. The air gauges and height gauges were used in combination to determine the average slopes of the surfaces with respect to the optical axis. The average slopes could be measured to better than 10 arc seconds. The torroidal test plate was used to determine the surface profile in planes passing through the optical axis. This test plate was fabricated from glass to the shape shown in Fig. 3-7a. When positioned on the optical surface as in Fig. 3-7b, such that close contact was made along the curve C, the deviations of the optical surface from the test plate surface along this curve could be determined from the configuration of the resulting interference fringes. The fabricator demonstrated, by comparison with flat and spherical reference surfaces, that the test plate profile along the curve C was correct to within 1/4 fringe (. 000003 in.). Deviations of the telescope profile from the test plate profile could be measured to better than . 000003 in. Because the saggittal depths of the paraboloidal and hyperboloidal sections differ by only 0. 000007 in., the same test plate could be used for both.

Lapping and polishing of telescope surfaces required approximately 4 months. The paraboloid was completed relatively quickly. However, as lapping proceeded on the hyperboloid, a large number of small crystalline inclusions were uncovered in the Kanigen layer. These protruded above the average surface, and perturbed the surface profile in their immediate vicinity. Because they were asymmetrically distributed about the hyperboloid, they also complicated the figuring operation. After unsuccessfully attempting to remove them with fine abrasives, the fabricator was forced to use a coarse abrasive which destroyed the existing surface finish. The finish was then restored; and, although some inclusions reappeared, the final polish is considered satisfactory. The completed telescope is shown in Fig. 3-8.

The results of the final acceptance tests are as follows:

	Paraboloid	Hyperboloid
Surface profile (deviation between optical surface and test plate surface).	0.00001 in.	0.00002 in.
Out-of-roundness	0.00005 in. T. I. R.	0.0001 in. T. I. R.
Error in the average slope	7 arc seconds	11 arc seconds
Error in diameter in the plane x = 0	.0066 in. over-size	.0035 in. over-size

Translational misalignment between axes of paraboloid and hyperboloid: .0015 in.

Angular misalignment between axes of paraboloid and hyperboloid: 40 arc seconds, maximum.

Error in focal length: approximately 0.15 in. longer than specified.

None of these errors was considered excessive or inconsistent with a design goal of 10 arc seconds angular resolution. The telescope was accepted from Diffraction Limited, Inc., on 3 August 1966.

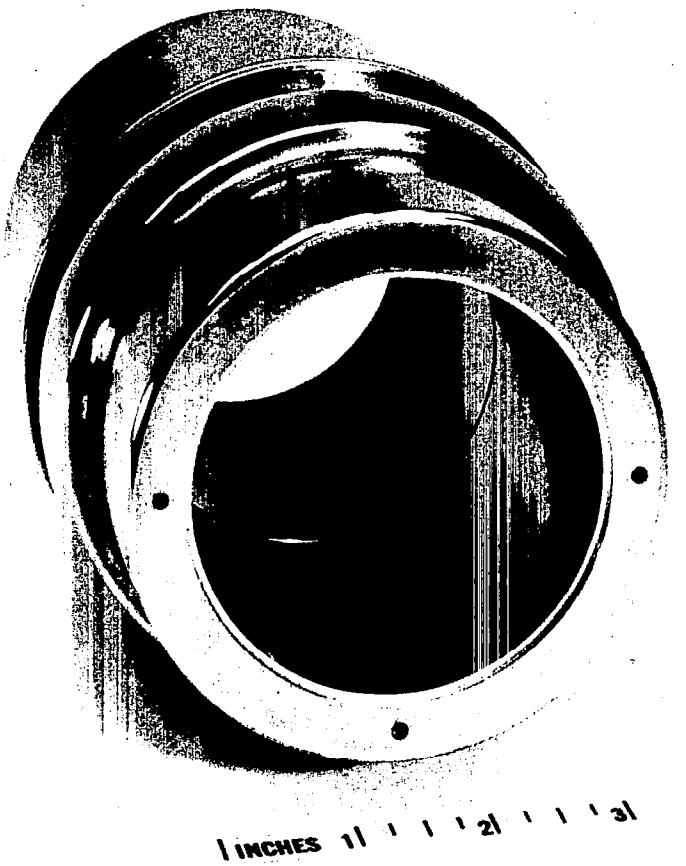

CQ-096

KANIGEN TELESCOPE

Fig. 3-8

4.0 Test and Calibration Techniques

Visible light and soft x-ray test and calibration techniques are described in this section. Most of the soft x-ray techniques discussed here were originated and developed in the course of this contract.

Specific tests performed on x-ray telescopes are presented in Section 5.0.

4.1 Visible Light Sources

During this contract, various visible light sources were used in conjunction with paraboloidal and flat mirrors, resolution patterns, and other optical components to test x-ray telescopes in the visible range. Routine optical methods were used to produce collimated beams and to simulate objects at infinity. Useful results of these tests are reported in Sections 2.4, 5.1.1, and 5.2.

One unique visible light test method was devised for accurately locating the focal surfaces of x-ray telescopes. Difficulty is often encountered in determining precisely where along the optical axis an image is sharpest. A less subjective method of focusing, employing a motor driven chopper wheel was sometimes used. An x-ray telescope was positioned in a collimated light beam and aligned to the beam axis. The telescope was then apertured such that only two regions of the annular opening, each about 30^{o} wide and positioned 180^{o} apart, were left open. A chopper wheel rotating at about one revolution per second was positioned in front of the telescope so as to alternately block off one of these regions and then the other. The image area was then examined with an eyepiece or a ground glass screen. The image typically would be seen to jump back and forth as the chopper rotated. Only when the plane of the ground glass or the focal plane of the eyepiece coincided with the position of best focus would the image be stationary. The technique is quite sensitive because of the ability of the eye to detect sudden small changes in position at the frequency at which the chopper wheel is driven. Besides its application to focusing, this

method may also be useful in precise measurements of the curvature of focal surfaces.

4.2 Variable Telescope Calibrator

A device called the variable telescope calibrator was constructed for measuring the reflection efficiencies of telescopes. The device was designed so that a tightly collimated x-ray beam of small cross-section could be directed upon a portion of the telescope entrance aperture. The telescope could be tilted so as to simulate any desired relation between the incident rays and the local telescope surface. The intensity of the resulting image was monitored with a geiger tube or recorded photographically. The telescope efficiency was calculated from the photographic data by scanning the image area with a microdensitometer and performing suitable integrations.

The variable telescope calibrator and its associated x-ray source are shown schematically in Fig. 4-1. The source is a modified Jarrell-Ash Microfocus Unit with its beryllium window removed. When in use, the calibrator and source were placed in a vacuum chamber separated from each other by 28 feet and pumped down to the 10^{-5} torr range. The source produced a divergent cone of rays, some of which were intercepted by a vertical slit 0.125 inches wide, which was positioned in front of the entrance aperture of the telescope being calibrated. Some of the rays passing through this slit impinged upon a part of the entrance aperture of the telescope. From the dimensions and spacing of the source and the slit, and from the width of the annular opening of the telescope, the divergence of these rays was calculated to be no more than 1.3 arc minutes.

As depicted in Fig. 4-1, the telescope and detector were mounted in a rigid frame. Let the calibrator axis be defined as that line which passes through the center C of the front aperture plate of the telescope and which is parallel to the ray path between the source and the telescope. The rigid frame was mounted so that it could be pivoted about the point C; and thus the telescope axis could be pivoted to make any desired angle θ with the collimator axis.

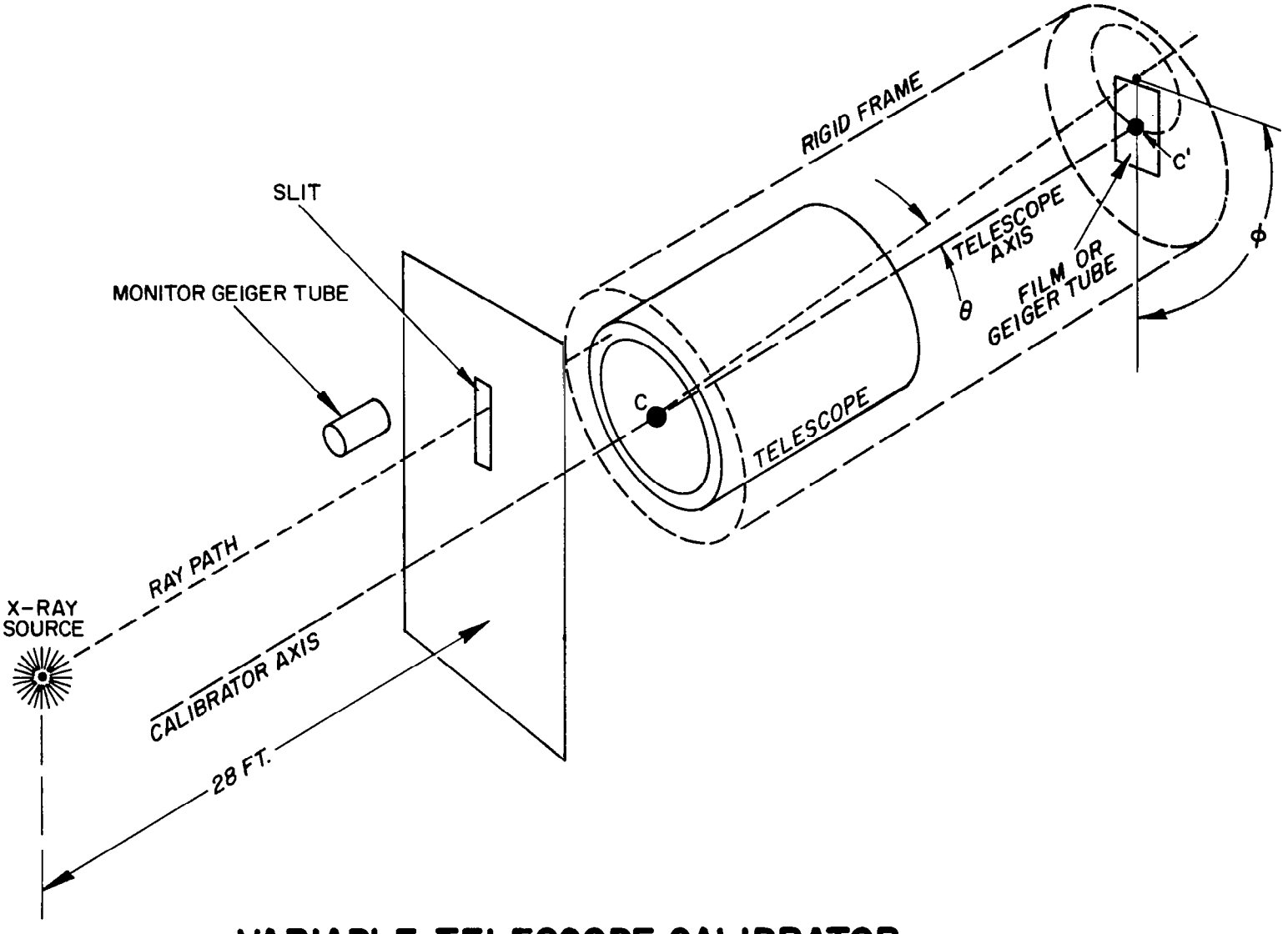

VARIABLE TELESCOPE CALIBRATOR

Fig. 4-1

(This motion was controlled by a rotary feed-through in vacuum system wall). In addition, the cylindrical frame could be pivoted about C such that the center of the film plane C traced out a circle centered on the calibrator axis. Thus, θ remained constant during this rotation. The point C could be held at any desired position angle ϕ on this circle. (This motion was produced by an electric motor which was controlled from outside the vacuum chamber).

The purpose of providing the calibrator with the degrees of freedom described above was to permit the establishment of various geometrical relations between the incident ray path and the telescope surface. It is obvious that the reflection efficiency of the telescope for a distant source which is off-axis by an angle θ could be measured by fixing the angle between the telescope axis and the calibrator axis at the value θ and then rotating the source and the slit together about the calibrator axis. The local reflection efficiencies, measured at several places during this rotation and suitably normalized over the rotation, would yield the reflection efficiency for such a source. However, it can be shown that this rotation is geometrically equivalent to holding the source and slit fixed and pivoting the rigid frame about C such that C traces out a circle, as shown in Fig. 4-1. That is, the sequence of angles made between the incident rays and the telescope surface will be the same for both motions. Two differences between these motions are as follows:

1. For the first motion, the complete telescope collecting area is scanned. For the second, the whole measurement is confined to a small portion of the collecting area.

2. The image point on the detector is stationary during the first motion, whereas it traces out a circle about C during the second.

The second motion, in which the source and slit are held stationary, was chosen in preference to the first for mechanical reasons.

In addition to the components mentioned above, the calibrator system included a geiger tube to monitor the source intensity and a shutter which could block the slit and open a direct path from the source to the film. The geiger tube was used to monitor the relative flux which produced each image point on the film. The telescope efficiencies were ultimately found by relating the densities of these dots to the integrated densitites of the reflected image points.

The source was operated at 3.0 or 4.0 KV, with a tube current of about 5 ma. An aluminum target was used for all exposures. The film was Ilford Industrial G X-ray film covered with. 0005 in. of aluminum. At a given angle θ between the telescope axis and the ray path, exposures were typically made for seven different values of ϕ . (Because of symmetry, it was sufficient to vary ϕ through a range of 180° instead of 360°.) The exposure time for each value of ϕ varied with source intensity, as monitored by the geiger tube. The average time was about 15 minutes. One of the resulting exposures is shown in Fig. 5-3. Microdensitometer scanning and analysis of telescope calibrator data are described in Section 5.1.2.

The estimated uncertainty in positioning θ was 1 arc minute; in ϕ , it was 1°.

Although this calibration technique proved feasible, and useful data was obtained, it had several obvious disadvantages:

1. It was tedious and time consuming to make the exposures and to reduce the data contained on them.

2. Measurements could be made on only a small portion of the telescope collecting area at a time.

3. The resulting data gives only very indirect information on the x-ray imaging properties and angular resolution of a telescope.

A potentially superior technique is presented in Section 4.3.

4.3 Multibeam Collimator

An improved test and calibration technique was developed to overcome the inconvenience and limitations of using x-ray beams of small cross-section to measure the performance of telescopes. The technique is based upon a device called the multibeam collimator, which can produce groups of highly collimated x-ray beams of large cross-section. Thus, it is most immediately applicable to measuring angular resolution. However, when used in conjunction with the pinhole array described in Section 4.4, measurements of reflection efficiency may also be possible with this collimator.

Collimated beams of x-rays can be produced by bundles of thin tubes or stacks of parallel plates. However, beam widths of less than 1^{o} are difficult to achieve in this manner. Finer beams can be produced by stacks of identical photoetched or electroformed grids; but the problem of alignment, such that the corresponding holes in all the grids lie along straight lines, greatly complicates the task of producing beams as fine as one arc minute. If, however, only two identical grids are used, this alignment problem is eliminated; and a type of collimation suitable for the testing of image forming x-ray optics can be obtained.

The multibeam collimator, shown schematically in Fig. 4-2, consists of two identical metal grids held parallel to each other, at a given spacing in a rigid frame. Each grid contains a large number of holes accurately placed in a regular 90^{o} array. A broad x-ray source is placed behind one of the grids so that a portion of the radiation can pass through the holes in the grids. Consider the rays passing through a given hole in grid A and the corresponding hole in grid B. Since the grids are identical, all such rays for all pairs of corresponding holes are parallel within an angle determined by the hole diameter and the grid spacing. (Let this parallel beam be called the axial beam). Similarly, since the spacing between holes is a constant, all rays passing through any given hole in grid A and the hole just above the

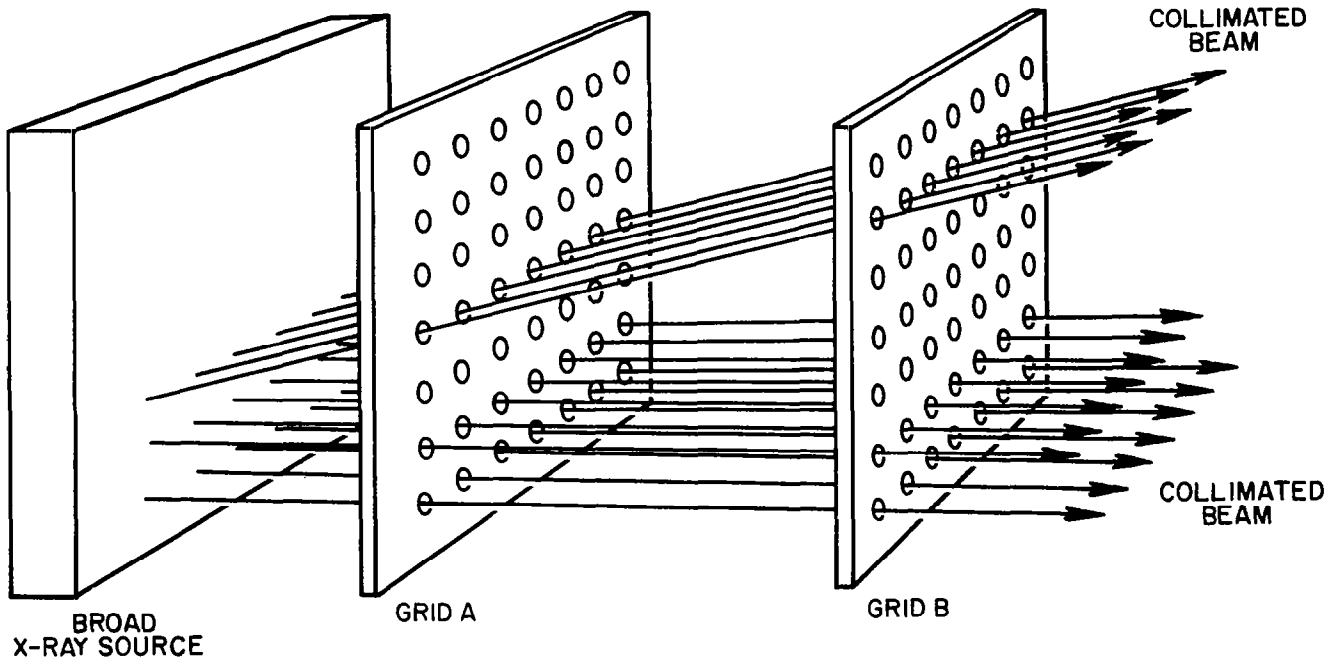

SCHEMATIC DIAGRAM OF THE MULTIBEAM COLLIMATOR

Fig. 4-2

CQ-099

...IMATOR AND X-RAY SOURCE

corresponding hole in grid B will also be parallel to each other. Considering many combinations of holes in the two grids, it can be seen that a large number of collimated beams will be generated. In fact, the collimator simulates a square array of point sources located at infinity. Note that the only critical alignment tolerance between the two grids is for rotations about the collimator axis. The degree of collimation and the spacial relation between the separate beams change quite slowly for all other rotations and translations.

A multibeam collimator and associated x-ray source were constructed for resolution tests on 3 inch telescopes (see Fig. 4-3). The two grids were held 18 inches apart in a cylindrical aluminum frame. Each grid contained approximately fifty thousand . 002 inch holes spaced . 016 in., center-to-center, in a square array. The tolerance in the positioning of the holes was . 0005 in., non-accumulative. For these values of hole diameter and spacing, the calculated angular width of each collimated beam is 0. 8 arc min., and the beams are separated from each other by 3 arc min.

The broad x-ray source is also shown in Fig. 4-3. A portion of the aluminum target, shaped like a truncated cone, can be seen through the opening in the source housing. Three concentric ring-shaped tungsten filaments, which do not show in this picture, are positioned near the conical surface of the target. In operation, the filaments are approximately at ground potential, and a positive high voltage is applied to the target. The electrons impinge on the conical surface of the target; and thus, from a point on the axis of the multibeam collimator, the emitting region appears to be an annular ring. This source is typically run at a beam current of 30 ma., at voltages up to 5 KV. The target is cooled with re-circulating distilled water.

4. 4 Pinhole Camera Array

It was found that a convenient method of measuring the reflection efficiency of an x-ray telescope is to compare its performance with that of a pinhole camera. Radiation from a uniform uncollimated source of large cross-section is allowed to fall simultaneously on the entrance aperture of the

telescope and on a pinhole camera array consisting of pinholes of various diameters. The resulting images from the telescope and the pinhole camera array are recorded on film. For a given exposure, the density of a photographic image is a function of the f-number of the device which produced the image. The f-numbers of the various elements of the pinhole camera are known from the pinhole diameters and the pinhole-to-film spacing. Thus, the effective f-number of the telescope (which is a function of the collecting area and the efficiency) can be found by comparing the density in the image which it produced with the densities of the pinhole camera images. Then from the known collecting area, the reflection efficiency can be found.

A pinhole camera array was constructed and used in several efficiency measurements made on electroformed telescopes. Thirteen holes with diameters ranging from . 0034 in. to . 027 in. were drilled in a single disk of . 003 in. brass. The thirteen separate images produced by the pinholes were recorded on a single piece of film placed 1. 75 inches behind the plane of the pinholes. Thus, the f-numbers of this pinhole camera array ranged from 65 to 515. The effective f-number of a typical electroformed telescope operating at 20% efficiency is about 120.

To insure that the x-ray intensity striking the pinholes was very nearly the same as that entering the telescope, the pinhole camera array was positioned on the telescope axis, against the front aperture plate. Its diameter was sufficiently small so that none of the collecting area of the telescope was shadowed.

A simple x-ray source consisting of a curved aluminum target and a single tungsten filament was placed on axis about 36 in. in front of the telescope. The x-ray flux from an area about 5 in. in diameter at the center of the target proved to be sufficiently uniform to yield useful data. The source was run at 2. 0 KV. Exposure times were about 2 hours. The exposed pieces of film from the pinhole camera array and the focal plane of the telescope were processed together in D-19. Data from several exposures

is discussed in Section 5. 1. 2.

This calibration technique is very convenient and fast compared to the use of collimated x-ray beams of small cross-section. (See Section 4. 2). Reduction of the data is especially simplified, since no integrations over the image area are required. Used in conjunction with a multibeam collimator, it may be possible to obtain the complete performance data (efficiency and angular resolution over the entire field of view) on a telescope from a single exposure.

5.0 Performance Testing of the X-ray Telescopes

In this section, the results of visible light and soft x-ray tests on the telescopes are presented. Due to the short period of time between the delivery of the Kanigen telescope and the completion of this contract, evaluation of this telescope was necessarily limited to visible light tests.

5.1 Tests Performed on Electroformed Nickel Telescopes

5.1.1 Visible Light Tests

In Fig. 2-9, a group of point light sources is resolved by an electroformed nickel telescope. However, because the geometry of image formation with conical optics, as discussed in Section 2.4, is particularly suited for use with point sources, a resolution test made with a pattern of such sources should not be considered conclusive. A resolution test pattern which is more suitable is shown in the lower part of Fig. 5-1. This pattern is a portion of the Air Force Resolution Target. The ability of an optical system to resolve the groups of parallel bars in this pattern is more indicative of the system's probable performance with, for instance, an intricately shaped solar x-ray source, than is its abiltiy to separate pairs of point sources.

The resolution target, mounted in a 35 mm. slide, was placed in the focal plane of a 12 inch diameter, 100 inch focal length paraboloidal mirror. The target was illuminated with a diffuse source. An electroformed nickel x-ray telescope was positioned and aligned in the resulting beam of light reflected from the mirror. Alignment was performed by pivoting the telescope until the image, as seen on a ground glass screen, was concentric with the ring of light that results from single reflections off the rear conical reflection surface. The image of the target, shown in the upper part of Fig. 5-1, was recorded on Polaroid Type 55 P/N film. The finest bar spacing which appears

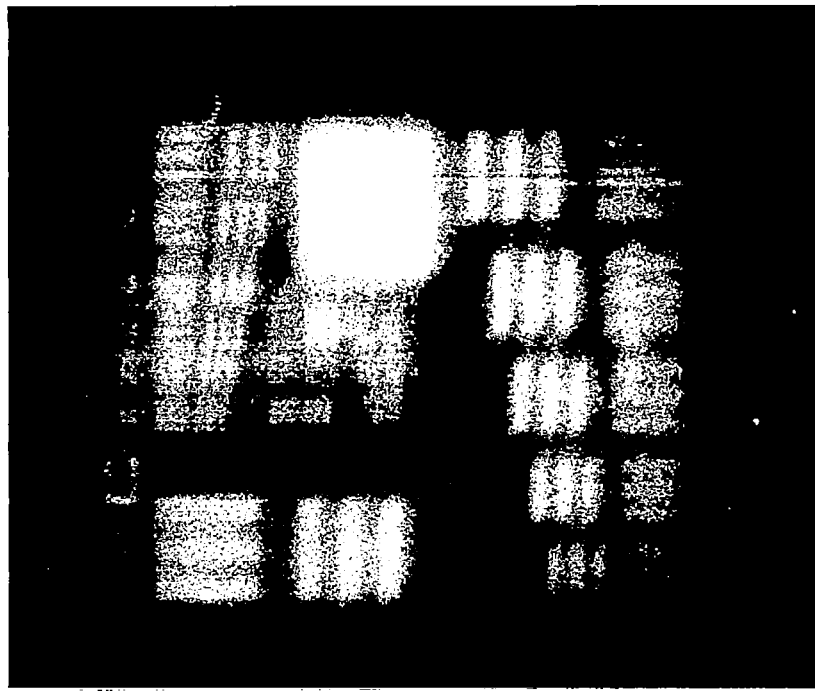

CQ-102

PHOTOGRAPH OF THE AIR FORCE RESOLUTION CHART TAKEN WITH AN ELECTROFORMED X-RAY TELESCOPE

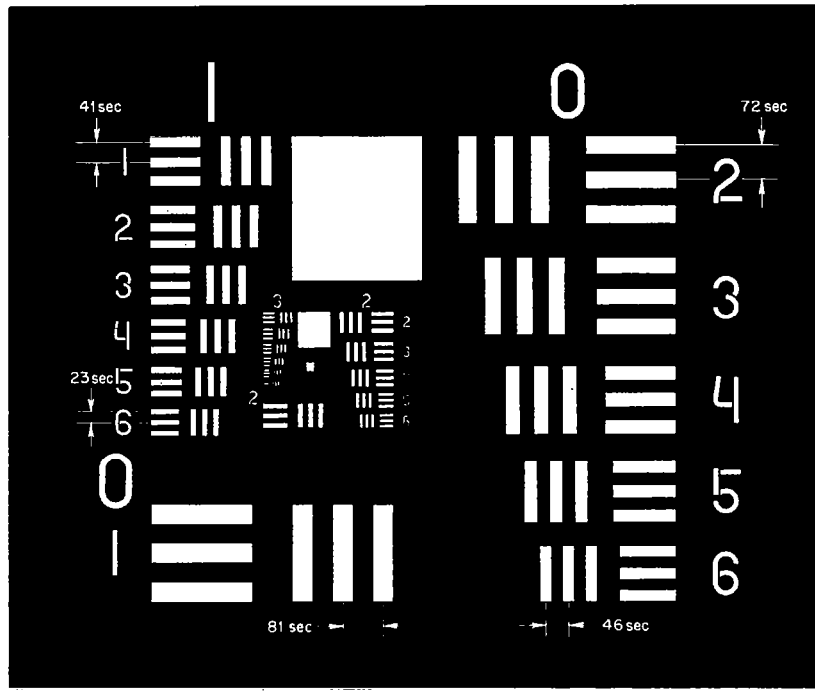

CQ-103

ENLARGEMENT OF THE RESOLUTION CHART, SHOWING ANGULAR SPACING OF SOME OF THE BAR GROUPS

Fig. 5-1

to be resolved is about 20 arc seconds, center to center. This compares with a calculated resolution, from Section 2-4, of 55 arc seconds. However, the contrast in the images of the finer bar groups is low. In order to compare the observed resolution with the calculated value, quantitative data on the intensity distribution in the image area would be necessary.

The telescope used to produce this exposure is considered to be a typical electroformed telescope. In the numerous tests using various targets that were performed during this contract, the performance of telescopes from various mandrels was very consistent.

5.1.2. Telescope Efficiency Measurements in the Soft X-ray Region

The telescope efficiency E at a given angle of incidence θ was defined as the ratio of the x-ray flux sent into the image of a distant point source, located at an angle θ from the optical axis, to the total flux from that source incident on the annular aperture of the telescope. Efficiency, so defined, includes the vignetting effects of the aperture plates as well as the variation of the reflection efficiency of the surfaces with θ.

An initial measurement of the efficiency of an electroformed nickel telescope was made using a geiger tube to detect the flux sent into the focal plane. The resulting curve is shown in Fig. 5-2. To produce each of the data points, the rigid frame of the variable telescope calibrator was set at the desired value of θ while ϕ was varied uniformly and continuously. (See Fig. 4-1). The total number of counts produced by the geiger tube in six complete rotations through ϕ were recorded. The telescope entrance aperture was then blocked and the direct path between the source and the geiger tube was opened to measure the incident flux. The efficiency E was calculated from the following relation:

$$E = \frac{C_t A_d}{C_d S \alpha L} \qquad (5\text{-}1)$$

where:

C_t = counting rate resulting from the radiation imaged in the focal plane, averaged over the revolutions through ϕ.

TELESCOPE EFFICIENCY
vs.
ANGLE OF INCIDENCE

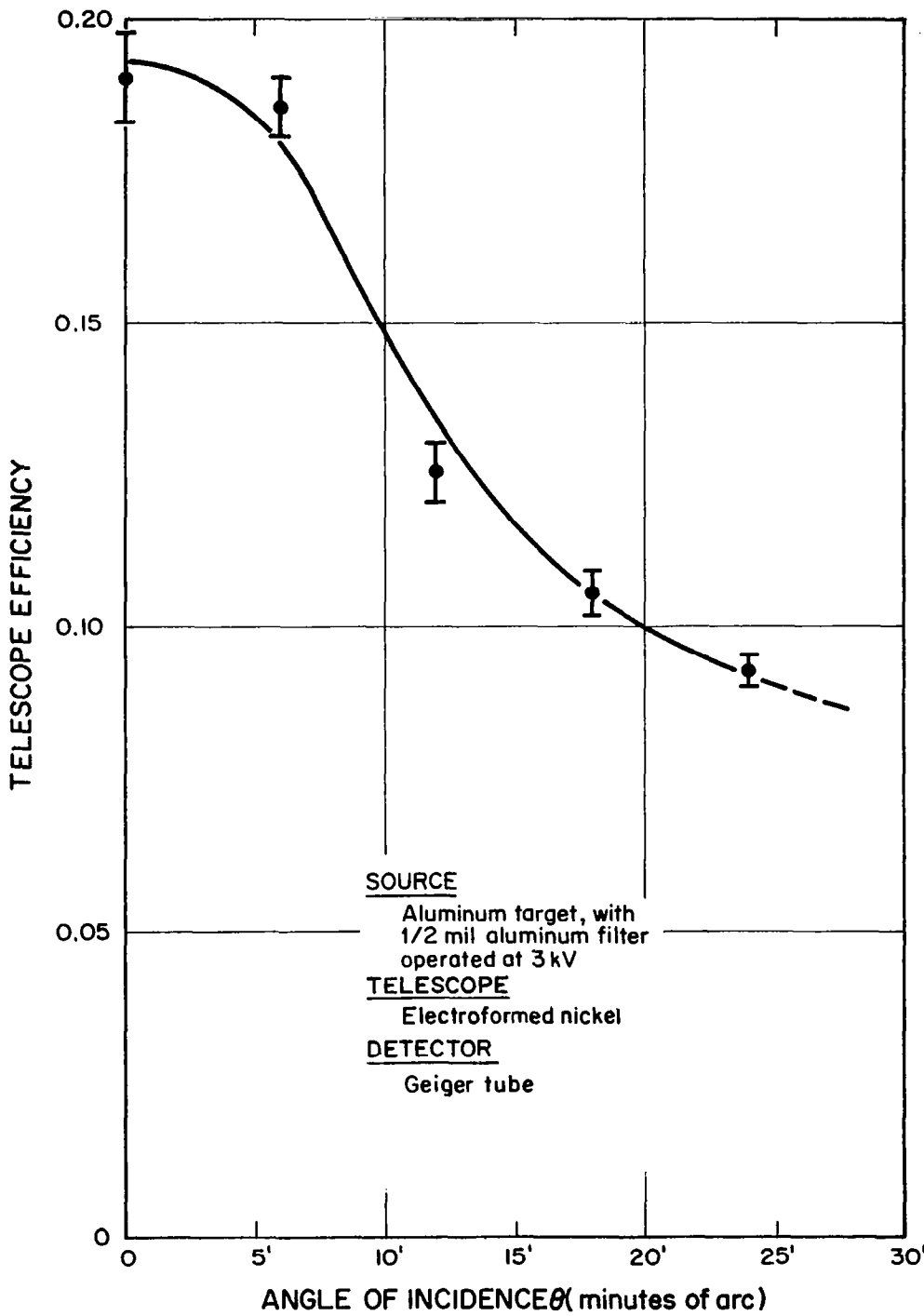

Fig. 5-2

A_d = cross-sectional area of the direct path to the source. (This was defined by a small circular aperture near the point C in Fig. 4-1).

C_d = counting rate observed when the direct path to the source was opened.

S = width of the slit placed in front of the telescope entrance aperture.

αL = annular opening of the telescope (Full-sized aperture plates were used).

The quantity $S\alpha L$ is the area of the portion of the annular aperture upon which the incident x-rays were allowed to fall. The source was run at 3.0 KV with an aluminum target, and was filtered with a .0005 in. thick aluminum foil. Thus, the incident radiation consisted primarily of the aluminum K line at 8.3A. The geiger tube window was 1.4 to 2 mg/cm^2 mica; its diameter was 1.1 in. Since these were relative measurements, it was not necessary to determine the efficiency of the geiger tube.

For later measurements of telescope efficiency, photographic film was substituted for the geiger tube in the focal plane. The primary reason for this was that the geiger tube counting rate was proportional to the total flux reflected into the focal plane, instead of to the flux which contributed to the effective image. Flux which was reflected with relatively large angular errors was included. Another reason was that the efficiency of the geiger tube was known to vary across its face. This variation could not simply be corrected in the experimental arrangement used for this measurement.

Fig. 5-3a is an enlargement of a typical exposure produced when photographic film (Ilford Industrial G X-ray film) was used as a detector in the focal plane. The image corresponding to $\theta = 0$ (radiation incident paraxially) is indicated by the arrow. Its asymmetrical shape is due to the fact that the telescope was apertured by the slit shown in Fig. 4-1. The seven images forming a semi-circle around it were produced by fixing the angle of incidence

CQ-098

(a)

CQ-100

(b)

VARIABLE TELESCOPE CALIBRATOR DATA

Fig. 5-3

θ at 12 arc minutes and stepping ϕ through seven different values in a 180^{o} range. The three images at the far right are for θ = 24 minutes. (The angle ϕ was stepped through a total of seven values at θ = 24 minutes. Due to vignetting by the aperture plates only three images were produced.) The circular areas in the upper part of the exposure are calibration dots, produced when the direct path to the source was opened for various lengths of time.

These exposures were made at a source voltage of 4.0 KV, in order to reduce the exposure time for each of the images. This was typically 15 minutes. An aluminum target was used.

The spreading of these images in the vertical direction is due to small scale slope errors in the reflecting surfaces. Substantial densities were recorded two to four arc minutes from the image centers, indicating slope errors of one to two arc minutes.

In order to calculate telescope efficiency from exposures such as Fig. 5-3a, microdensitometer scans of the image areas were produced. Scanning was done on a modified Joyce-Loebel densitometer. The scan of the image indicated by the arrow in Fig. 5-3a is reproduced in Fig. 5-3b. The scanning element was $81\mu \times 81\mu$, which is small compared to the details of interest in the original image. Fig. 5-3b can be considered to be a contour map of the photographic density in the image area. The contours were drawn on this scan, and the areas between adjacent contour lines (regions of equal density) were measured with a planimeter. The telescope efficiency was then calculated as follows:

$$E = \frac{\sum_i P_i}{C_m K S \alpha L} = \frac{\sum_i F(D_i) a_i}{C_m K S \alpha L} \qquad (5\text{-}2)$$

where:

$\sum_i P_i$ = summation over the image area of the number of photons P_i imaged in each contour interval i.

C_m = counts registered by the monitor geiger tube (see Fig. 4-1) while the image was produced.

K = monitor geiger tube calibration constant (the ratio between the number of photons per unit area per unit time incident on the geiger tube and the number of counts registered per unit time).

$F(D_i)$ = film calibration function. (The number of photons per unit area necessary to produce a density D_i).

a_i = area of the contour interval i whose density is D_i.

(The quantities S and αL were previously defined for Equation 5-1). It was not necessary to measure K, or find the absolute film calibration function F(D). A relative film calibration curve f(D) was constructed using the calibration dots. This consisted of a plot of the density of each calibration dot, as measured with the densitometer, versus the number of counts registered by the monitor geiger tube while the dot was produced. Thus:

$$F(D) = Kf(D) \tag{5-3}$$

Substituting this into Equation 5-2, the geiger tube calibration constant cancels. The resulting expression for telescope efficiency is:

$$E = \frac{\sum_i f(D_i) a_i}{C_m S \alpha L} \frac{d^2}{(d+F)^2} \tag{5-4}$$

Here, $d^2/(d + F)^2$ is a geometrical factor to correct for the fact that the monitor geiger tube was closer to the source by a distance F than was the film. The distance d is the spacing between the source and the telescope (28 ft.); F is the focal length of the telescope (33 in.).

The choice of the image area over which the summation of $f(D_i)\, a_i$ is carried out is somewhat arbitrary. For the scan shown in Fig. 5-3b, two different calculations were performed. The first was a summation over the area within the circle shown on the scan. This circle is concentric with the apparent image center (the point of maximum density). Its diameter corresponds to the angle $\alpha L/F$ (3.5 arc min.) in the focal plane of the telescope. This value was chosen because it is the calculated angular diameter of the image of a distant point source, as formed by a perfect conical system (see Section 2.4). The resulting telescope efficiency E was 16%. This efficiency can be considered to apply to a source on axis whose angular diameter is smaller than $\alpha L/F$. The second summation was over the entire area for which the microdensitometer detected a density above the background level. This area corresponds to

1.5 arc min. by 15 arc min. The resulting telescope efficiency E was 27%. This efficiency can be considered to apply to an extended source (angular diameter large compared to the $\alpha L/F$)on axis.

Summations over the entire areas with densities above background were performed on the seven images for θ = 12 minutes, shown in Fig. 5-3a. The resulting efficiencies were normalized over $\emptyset$ to give a net efficiency of 17% for a broad source 12 minutes off axis.

Telescope efficiency measurements were also made using the broad x-ray source and pinhole camera array described in Section 4.4. Exposures were made at a source voltage of 2.0 KV; an aluminum target was used. A total of four exposures were made on electroformed nickel telescopes using Ilford Industrial G X-ray film. The average density above background of the image produced by each pinhole in the array was then plotted against the corresponding f-number for that pinhole. The density measurements were made with a MacBeth Quantalog TD-100 densitometer. Using the resulting curve and the measured net density at a selected point within the image formed by the telescope, the effective f-number of the telescope for the angle of incidence θ corresponding to that point was found. The effective collecting area A_{eff} for this value of θ was then calculated using the following expression:

$$A_{eff} = \pi\left(\frac{F}{2f_{eff}}\right)^2 \qquad (5-5)$$

where f_{eff} is the effective f-number. The telescope efficiency E is the ratio between A_{eff} and the actual area of the entrance aperture of the telescope (2.04 cm^2). The resulting values of E ranged from 22% for paraxial radiation to 13% for θ = 24 arc min.

The reflection efficiencies measured by the pinhole camera technique and by the other methods described in this section are summarized in Table I. Comparisons between the values of E found by these methods are difficult to make because:

1. Different source voltages were used, resulting in different

Calibration Device	Image Area Included in Summation	Detector	Source Voltage	TELESCOPE EFFICIENCY (percent) θ = 0	θ = 6 min.	θ = 12 min.	θ = 18 min.	θ = 24 min.
Variable telescope calibrator	Total Focal Plane	Mica window geiger tube	3.0 KV	19	18	13	11	9
Variable telescope calibrator	Area within a circle of diameter $\alpha L/F$ (3.5 min.) around image center	Ilford Industrial G X-ray film	4.0 KV	16	--	--	--	--
Variable telescope calibrator	Total area of observable photographic density	Ilford Industrial G X-ray film	4.0 KV	27	--	17	--	--
Pinhole camera array with broad x-ray source	Area large compared to a circle of diameter $\alpha L/F$	Ilford Industrial G X-ray film	2.0 KV	22	22	20	17	13

TABLE I

Summary of electroformed nickel telescope efficiency measurements.
(An aluminum x-ray target was used for all measurements)

x-ray spectral distributions.

2. Detectors with different spectral response curves were employed.

3. The measurements included to varying degrees the diffusely reflected radiation which intersected the focal plane outside the effective image area.

Using the pinhole camera technique, a measurement was made of the efficiency of a nickel telescope whose reflecting surfaces were covered with a 500A evaporated gold layer. The source voltage was 2.0 KV. The resulting on-axis efficiency is 7.8%. That the efficiency of a telescope with gold reflecting surfaces should be lower than one with nickel surfaces is, in this wavelength region, consistent with the reflection efficiency calculations in Section 2.2.

5.1.3. Multibeam Collimator Test

Fig. 5-4 is a photograph of a simulated array of x-ray sources at infinity taken with an electroformed nickel telescope. The center-to-center spacing of these sources was 3 arc min. The array was produced by the multibeam collimator described in Section 4.3. The source voltage was 4.0 KV. Ilford Industrial G X-ray film, processed in D-19, was used. The exposure time was 11 hours at an average source current of 25 ma.

Using the known hole diameter (.002 in.) and grid spacing (18 in.), the calculated divergence of each of the x-ray beams produced by this collimator is 0.8 arc min. The apparent diameter of the separate images in Fig. 5-4 is about one arc minute. Thus, the combined effects of the errors in positioning of the holes in the collimator grids (on the order of .0005 in.), and the imperfect focusing properties of the telescope have produced only a small increase in the image size. The magnitude of this increase indicates a telescope resolution of about 30 arc seconds in the soft x-ray range.

The decrease in density of the images with distance from the center of this photograph is due partly to the vignetting properties of the telescope, and partly to the 25 ft. separation between the telescope and multibeam col-

MULTIBEAM COLLIMATOR EXPOSURE TAKEN WITH ELECTROFORMED TELESCOPE

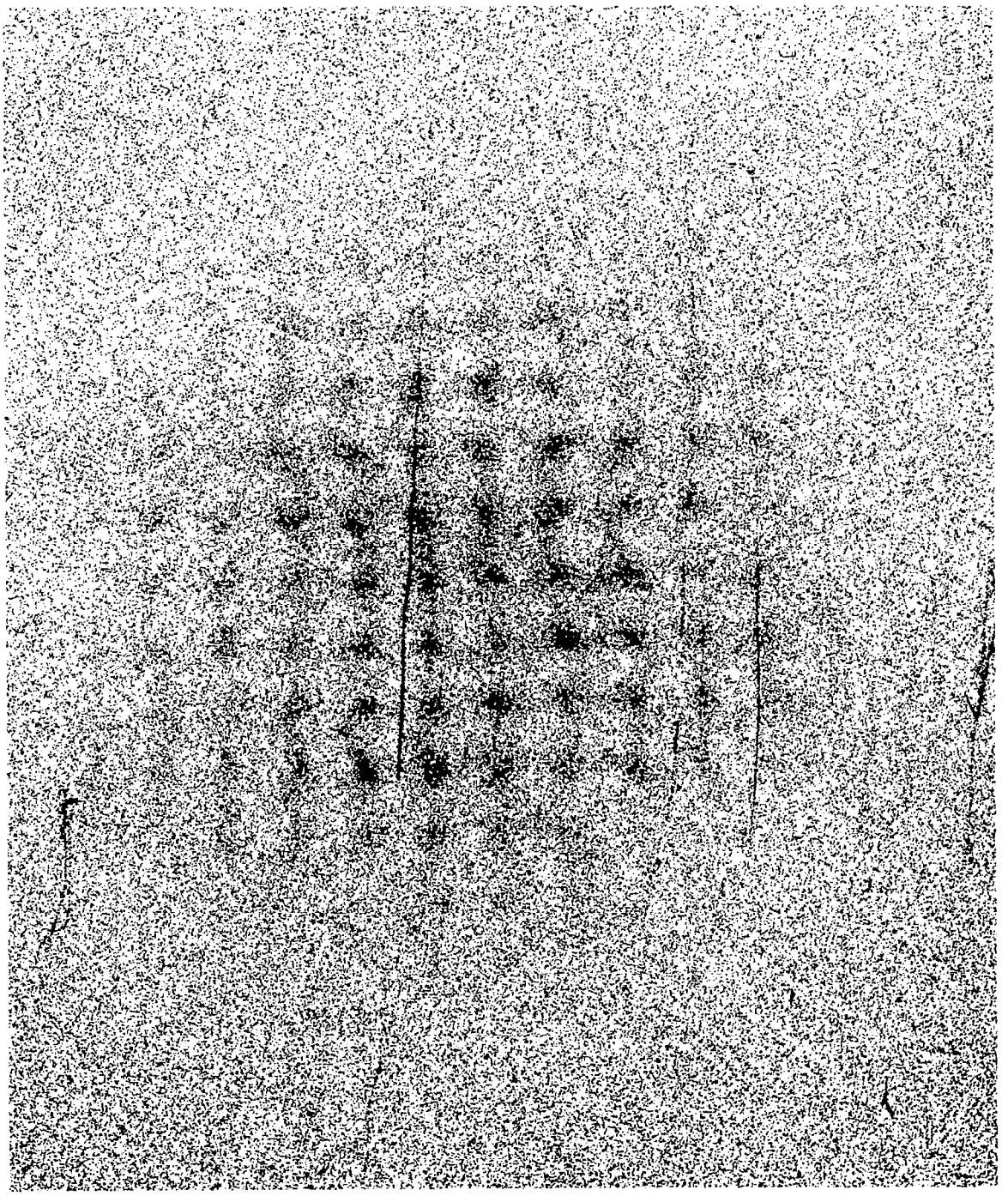

CQ-001

Fig. 5-4

limator.

5. 1. 4. Vacuum And Thermal Testing

Several of the electroformed telescopes fabricated under this contract have been subjected to extended periods of vacuum environment. Typical pressures were in the 10^{-5} torr range. Mirrors have remained at this pressure with no detectable change in reflection efficiency. One particular mirror was maintained in a vacuum for 5 weeks, during which time reflection efficiency measurements were performed. There was no observable degradation in reflection efficiency or surface quality in any of the tests due to prolonged exposure to a vacuum environment.

A number of the telescopes were also subjected to thermal cycling from $-10^{o}C$ to $+40^{o}C$. Mechanical strains were introduced into these telescopes due to a differential thermal expansion between the aperture plate and the mirror. A satisfactory solution to this problem has been obtained under Contract NAS 5-3569. On this program, the electroformed mirror which is used in the OSO-D X-ray Telescope Experiment is cushioned by a layer of RTV 602 Silicon Rubber inside a holding cylinder. Using this method, no distortion was introduced by the vibration or thermal environment which was required for experiment qualification.

5. 2 Visible Light Test of the Kanigen Telescope

A visible light photograph of a portion of the Air Force Resolution Target made with the Kanigen Telescope is reproduced in the left half of Fig. 5-5. The test setup is the same as that described in Section 5. 1. 1, except that microscope optics were used to magnify the image before it was projected on the film. This was done because film grain size and grain clumping blurred the finer details of the image when the film was placed directly in the focal plane. Kodak High Contrast Copy film was used for this exposure.

Bar groups with center-to-center spacings of less than 5 arc seconds are definitely resolved. Bars spaced less than 3 arc seconds center-to-center are imaged separately, at low contrast. Thus, the design goal of 10 arc

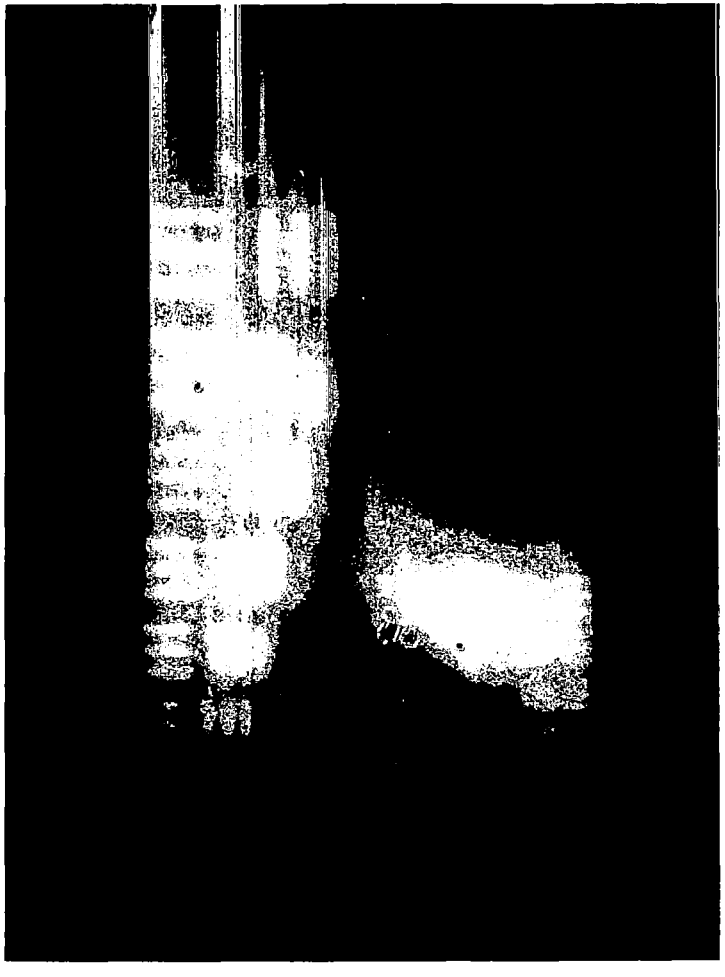

CQ-095

PHOTOGRAPH OF THE AIR FORCE RESOLUTION CHART TAKEN WITH THE KANIGEN-COATED X-RAY TELESCOPE

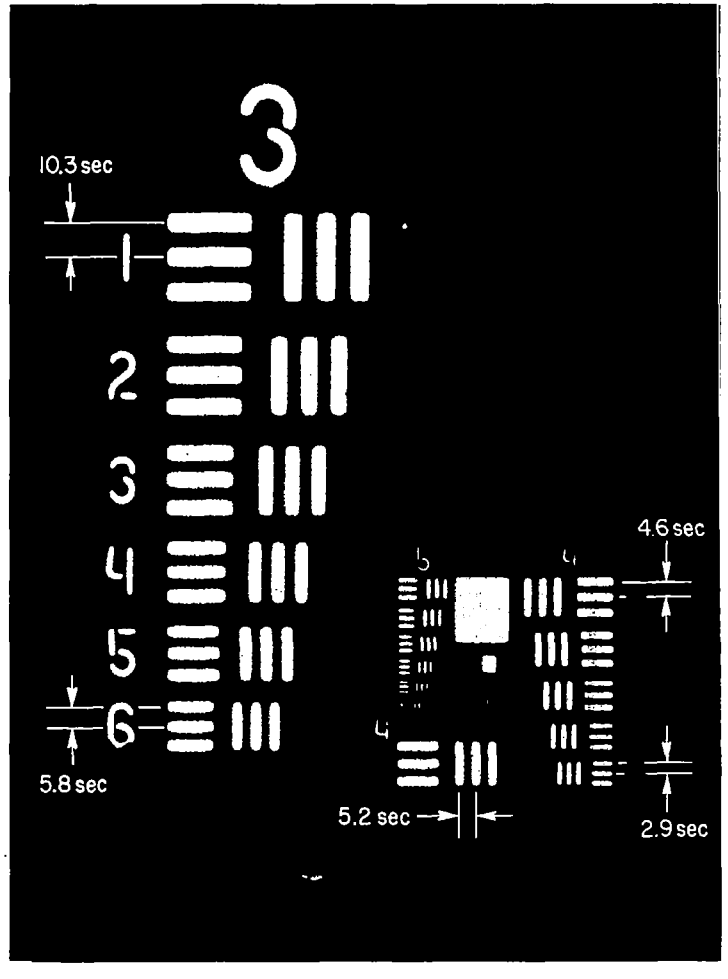

CQ-097

ENLARGEMENT OF THE RESOLUTION CHART, SHOWING ANGULAR SPACING OF SOME OF THE BAR GROUPS

Fig. 5-5

seconds resolution was exceeded for tests in the visible range.

The angular resolution obtained with the Kanigen telescope is approximately an order of magnitude improvement over that of the electroformed telescopes. The improved resolution indicates that the magnitude of the local slope errors is smaller for this telescope; and thus it is expected that its efficiency will also be found to be higher than that of the electroformed telescopes. This is because fewer rays will be reflected entirely out of the image area by surface irregularities; and fewer rays will strike other irregularities that are pitched beyond the critical angle of reflection θ_c, and be absorbed.

APPENDIX A

Ray Tracing Procedure

The incident rays were expressed as vectors. (See Fig. A-1). A reflected ray vector corresponding to the reflection of a given incident ray vector off of a chosen point P_1 on the surface S_1 of the paraboloid was found by the following operation:

$$\bar{R}_2 = \bar{R}_1 - 2\frac{(\bar{R}_1 \cdot \bar{\nabla}S_1)}{|\bar{\nabla}S_1|}\frac{\bar{\nabla}S_1}{|\bar{\nabla}S_1|} \qquad \text{(A-1)}$$

where:

$\bar{R}_1$ = incident ray vector

$\bar{R}_2$ = reflected ray vector

$\bar{\nabla}S_1$ = The outward normal to the paraboloid at the point of reflection P_1.

An analytic expression was found for the line parallel to $\bar{R}_2$ and passing through P_1. Then, the intersection point P_2 of this line with S_2, the surface of the hyperboloid, was found. Then, performing an operation at P_2 similar to that given in Equation A-1, the ray vector $\bar{R}_3$ after reflection off the hyperboloid was found. Finally the coordinates of the intersection of the focal surface with the line parallel to $\bar{R}_3$ and passing through P_2 were found. Let this striking point be P_3.

Five incident ray vectors R_1 were chosen, corresponding to angles of 0, 5, 10, 15 and 20 arc minutes from the optical axis. Each R_1 was traced through the system, by the procedure outlined above, for sixty different striking points P_1 on the paraboloid. The coordinates of the sixty

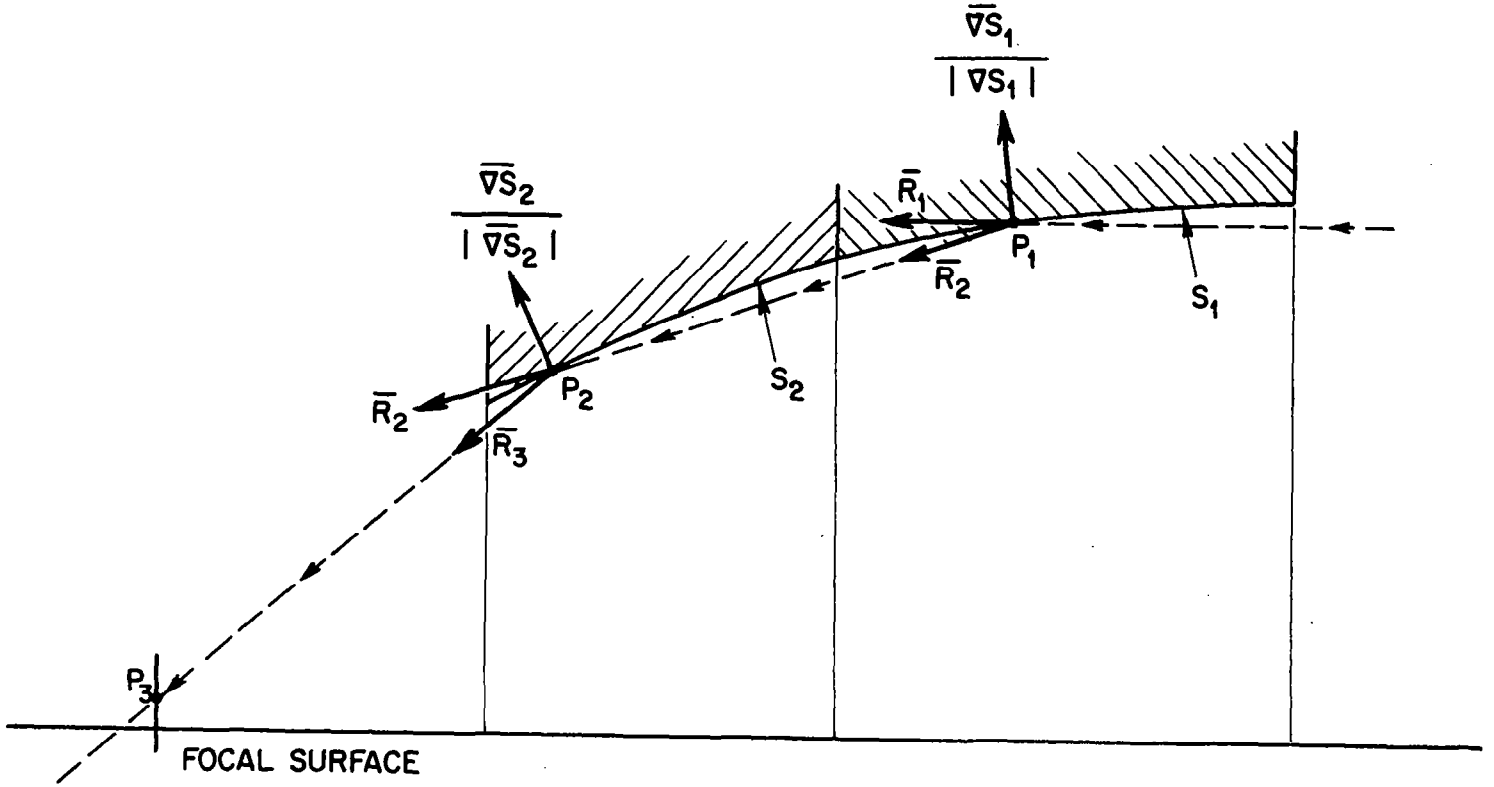

GEOMETRY OF THE RAY TRACING PROCEDURE

Fig. A-1

corresponding points P_3 on the focal surface were used to produce the blur circle plot for each incident ray vector R_1. For each computer run, then, a total of 300 rays were traced.

APPENDIX B

Definition of Angular Resolution

In calculating the intensity profiles in images of distant point sources formed by grazing incidence optical systems, $1/r$ distributions are encountered. Because of this, such a system should in principle be able to separate two arbitrarily close points sources, until the modification in the $1/r$ distributions resulting from diffraction becomes important. In practice, however, resolution in the X-ray range is limited to much larger angles by fabrication tolerances and instrument jitter. In addition, some sources of interest are not points. Thus, in order that calculations of angular resolution will yield more realistic results, another definition of angular resolution has been adopted.

So defined, resolution is the minimum angular separation of two semi-infinite sources for which image intensity still drops to half-maximum midway between the sources. Thus, in Figure A-2, the cross-hatched regions A and B are images of the semi-infinite sources as formed by a perfect imaging system. The resolution of a real system is δ/F (where F is the focal length) if the intensity along line J is just half that in those regions of A and B which are far from J.

Let the radius of the $1/r$ intensity distribution in the image of a point source be r_o, beyond which the intensity is zero. Then, since the two semi-infinite sources can be considered to be made up of many point-like source elements, the intensity at point P on line J is:

$$I(P) = 4\int_n^m \int_t^s \frac{K}{r} r\,dr\,d\theta \qquad \text{(B-1)}$$

GEOMETRY FOR THE DEFINITION OF ANGULAR RESOLUTION

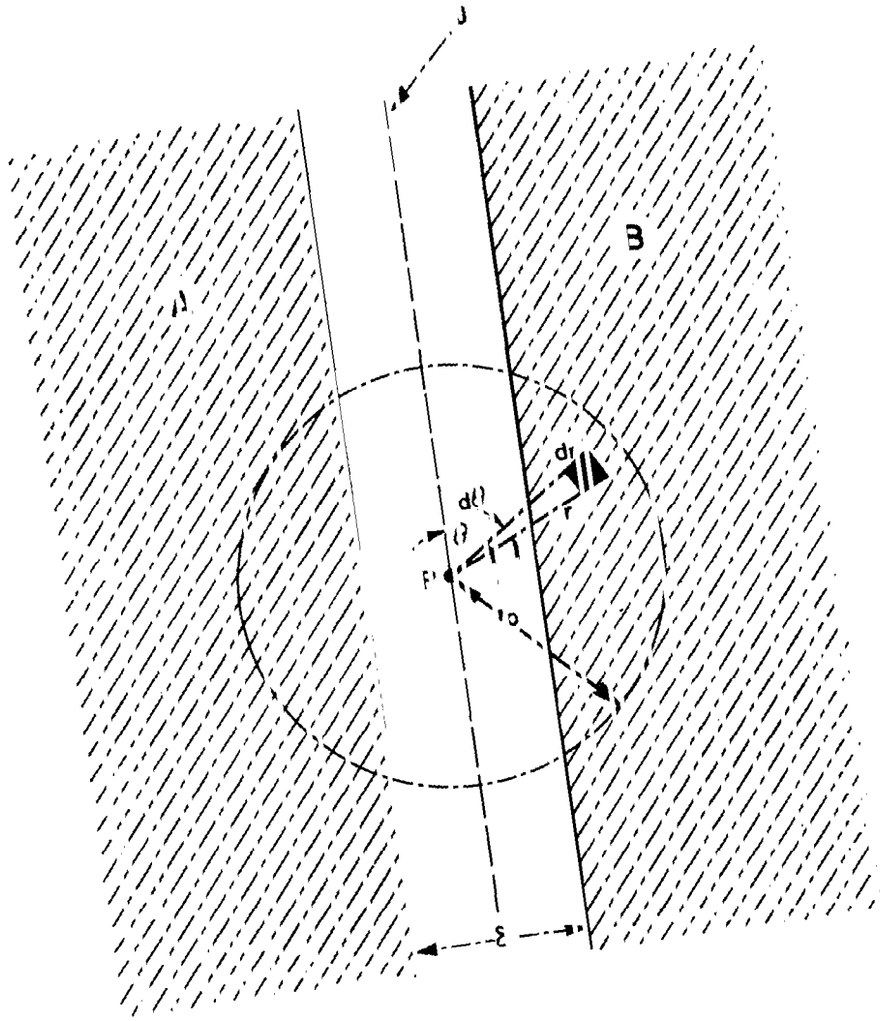

Fig. A-2

where:

$$m = \cos^{-1}\left(\frac{\delta}{2r_o}\right)$$

$$n = 0$$

$$s = r_o$$

$$t = \frac{\delta}{2\cos\theta}$$

$$K = \text{constant}$$

This becomes:

$$I(P) = 4K\left[r_o \cos^{-1}\left(\frac{\delta}{2r_o}\right) + \frac{\delta}{2}\log\left(\frac{r_o + \frac{\delta}{2} - \left[r_o^2 - \frac{\delta^2}{4}\right]^{1/2}}{r_o + \frac{\delta}{2} + \left[r_o^2 - \frac{\delta^2}{4}\right]^{1/2}}\right)\right] \qquad \text{(B-2)}$$

When this expression for I(P) is equated to $\pi r_o K$ (that is, one-half the intensity in those regions of A and B which are very far from line J), the resulting solution is:

$$\delta = 0.52 r_o \qquad \text{(B-3)}$$

(This solution was found graphically). Thus, using this definition:

$$\text{Angular Resolution} = \delta/F = \frac{0.52 r_o}{F} \qquad \text{(B-4)}$$

REFERENCES

1. R. Giacconi and B. Rossi, J. Geophys. Res. 65 , 773 (1960).

2. H. Wolter, Ann. Physik 10, 94 (1952).

3. R. Giacconi, N. F. Harmon, R. F. Lacey, Z. Szilagyi, J. Opt. Soc. Am. 55 , 345 (1965).

4. A. Compton and S. Allison, X-rays in Theory and Experiment, (D. Van Nostrand Company, New York, 1935), p. 305-310.

5. B. Henke, R. White and B. Lundberg, J. Appl. Phys. 28 , 98 (1957).

6. B. Henke in Advances in X-ray Analysis, W. Mueller, G. Mallett and M. Fay, Eds. (Plenum Press, New York, 1964), p. 460.

7. W. Reidy, et al, "Phase I Final Report for Engineering Model of X-ray Optical Systems For the Advanced Orbiting Solar Observatory", Contract NAS 5-9041. American Science and Engineering, Final Technical Report, ASE-2090, Feb. (1966).

8. M. Born and E. Wolf, Principles of Optics, (MacMillan Company, New York, 1964), p. 416.

9. R. Giacconi, W. P. Reidy, T. Zehnpfennig, J. C. Lindsay and W. S. Muney, Astrophys. J. 142 , 1274 (1965).

October 1966
American Science and Engineering, Inc.
11 Carleton Street
Cambridge, Massachusetts 02142